



This is a repository copy of *MET currents and otoacoustic emissions from mice with a detached tectorial membrane indicate the extracellular matrix regulates Ca²⁺ near stereocilia*.

White Rose Research Online URL for this paper:
<https://eprints.whiterose.ac.uk/172574/>

Version: Published Version

Article:

Jeng, J, Harasztosi, C, Carlton, A.J. orcid.org/0000-0002-1054-3901 et al. (8 more authors) (2021) MET currents and otoacoustic emissions from mice with a detached tectorial membrane indicate the extracellular matrix regulates Ca²⁺ near stereocilia. *The Journal of Physiology*, 599 (7). pp. 2015-2036. ISSN 0022-3751

<https://doi.org/10.1113/jp280905>

Reuse

This article is distributed under the terms of the Creative Commons Attribution (CC BY) licence. This licence allows you to distribute, remix, tweak, and build upon the work, even commercially, as long as you credit the authors for the original work. More information and the full terms of the licence here:
<https://creativecommons.org/licenses/>

Takedown

If you consider content in White Rose Research Online to be in breach of UK law, please notify us by emailing eprints@whiterose.ac.uk including the URL of the record and the reason for the withdrawal request.



eprints@whiterose.ac.uk
<https://eprints.whiterose.ac.uk/>

MET currents and otoacoustic emissions from mice with a detached tectorial membrane indicate the extracellular matrix regulates Ca^{2+} near stereocilia

Jing-Yi Jeng¹, Csaba Harasztosi² , Adam J. Carlton¹ , Laura F. Corns¹, Philine Marchetta², Stuart L. Johnson^{1,3}, Richard J. Goodyear⁴ , Kevin P. Legan⁴ , Lukas Rüttiger² , Guy P. Richardson⁴  and Walter Marcotti^{1,3} 

¹Department of Biomedical Science, University of Sheffield, Sheffield, UK

²Department of Otolaryngology Head & Neck Surgery, THRC, University of Tübingen, Tübingen, 72076, Germany

³Neuroscience Institute, University of Sheffield, Sheffield, S10 2TN, UK

⁴School of Life Sciences, Falmer, University of Sussex, Brighton, BN1 9QG, UK

Edited by: Kim Barrett & Ian Forsythe

Key points

- The aim was to determine whether detachment of the tectorial membrane (TM) from the organ of Corti in *Tecta/Tectb*^{-/-} mice affects the biophysical properties of cochlear outer hair cells (OHCs).
- *Tecta/Tectb*^{-/-} mice have highly elevated hearing thresholds, but OHCs mature normally.
- Mechanoelectrical transducer (MET) channel resting open probability (P_o) in mature OHC is ~50% in endolymphatic $[\text{Ca}^{2+}]$, resulting in a large standing depolarizing MET current that would allow OHCs to act optimally as electromotile cochlear amplifiers.
- MET channel resting P_o *in vivo* is also high in *Tecta/Tectb*^{-/-} mice, indicating that the TM is unlikely to statically bias the hair bundles of OHCs.
- Distortion product otoacoustic emissions (DPOAEs), a readout of active, MET-dependent, non-linear cochlear amplification in OHCs, fail to exhibit long-lasting adaptation to repetitive stimulation in *Tecta/Tectb*^{-/-} mice.
- We conclude that during prolonged, sound-induced stimulation of the cochlea the TM may determine the extracellular Ca^{2+} concentration near the OHC's MET channels.

Abstract The tectorial membrane (TM) is an acellular structure of the cochlea that is attached to the stereociliary bundles of the outer hair cells (OHCs), electromotile cells that amplify motion of the cochlear partition and sharpen its frequency selectivity. Although the TM is essential for hearing, its role is still not fully understood. In *Tecta/Tectb*^{-/-} double knockout mice, in which the TM is not coupled to the OHC stereocilia, hearing sensitivity is considerably reduced compared with that of wild-type animals. *In vivo*, the OHC receptor potentials, assessed using cochlear microphonics, are symmetrical in both wild-type and *Tecta/Tectb*^{-/-} mice, indicating that the TM does not bias the hair

Jing-Yi Jeng received her MSc degree in Biotechnology at National Tsing Hua University (Taiwan) and her PhD in Biomedical Science at The University of Sheffield (UK). Her research aims to understand the physiological mechanisms crucial for the development and ageing of the cochlear hair cells in the mammalian cochlea. She is a Postdoctoral Research Associate within the Hearing Research Group (<https://www.sheffield.ac.uk/hearing>) in the Department of Biomedical Science at The University of Sheffield (UK).



bundle resting position. The functional maturation of hair cells is also unaffected in *Tecta/Tectb*^{-/-} mice, and the resting open probability of the mechano-electrical transducer (MET) channel reaches values of ~50% when the hair bundles of mature OHCs are bathed in an endolymphatic-like Ca²⁺ concentration (40 μM) *in vitro*. The resultant large MET current depolarizes OHCs to near -40 mV, a value that would allow optimal activation of the motor protein prestin and normal cochlear amplification. Although the set point of the OHC receptor potential transfer function *in vivo* may therefore be determined primarily by endolymphatic Ca²⁺ concentration, repetitive acoustic stimulation fails to produce adaptation of MET-dependent otoacoustic emissions *in vivo* in the *Tecta/Tectb*^{-/-} mice. Therefore, the TM is likely to contribute to the regulation of Ca²⁺ levels around the stereocilia, and thus adaptation of the OHC MET channel during prolonged sound stimulation.

(Received 2 October 2020; accepted after revision 3 February 2021; first published online 9 February 2021)

Corresponding authors L. Rüttiger: Department of Otolaryngology Head & Neck Surgery, THRC, University of Tübingen, 72076 Tübingen, Germany. Email: lukas.ruettiger@uni-tuebingen.de

G. P. Richardson: School of Life Sciences, University of Sussex, Falmer, Brighton BN1 9QG, UK. Email: g.p.richardson@sussex.ac.uk

W. Marcotti: Department of Biomedical Science, University of Sheffield, Sheffield, UK. Email: w.marcotti@sheffield.ac.uk

Introduction

The tectorial membrane (TM) is a strip of extracellular matrix that lies atop of the organ of Corti (Fig. 1A). It is attached medially to the spiral limbus and laterally to the tips of the hair bundles of the outer hair cells (OHCs), electromotile cells that can amplify the motion of the basilar membrane at low sound pressure levels and sharpen its frequency selectivity (Dallos, 1992; Ashmore, 2018). The electromotility of OHCs, the rapid voltage-dependent contractions of the basolateral membrane uniquely due to the presence of the motor protein prestin, a modified anion exchanger (Zheng *et al.* 2000; Liberman *et al.* 2002), form the basis of the so-called cochlear amplifier. The TM is known to be essential for normal hearing and has been proposed to play a number of roles (Lukashkin *et al.* 2010). There is evidence that it acts as an inertial mass that can influence the timing and gain of the cochlear amplifier (Mammano & Nobili, 1993; Gummer *et al.* 1996; Legan *et al.* 2000). Furthermore, it ensures that the stereociliary bundles of the inner hair cells (IHCs), which are not coupled directly to the TM, are displaced by fluid flow in the sub-tectorial space (Legan *et al.* 2005; Nowotny & Gummer, 2006). More recently, the TM has been shown to stabilize the cochlear amplifier (Cheatham *et al.* 2018), and that it may act as a source of Ca²⁺ required for mechano-electrical transduction and thus able to modulate the ionic environment around the hair-cell stereocilia (Strimbu *et al.* 2019).

In *Tecta*^{ΔENT/ΔENT} mice with a functional-null mutation in *TECTA*, a major non-collagenous component of the TM, the TM fails to form correctly and is no longer associated with the apical surface of the organ of Corti (Fig. 1B; see also Legan *et al.* 2000). The hearing thresholds in *Tecta*^{ΔENT/ΔENT} mutant mice are

considerably elevated compared with those recorded in wild-type mice. Importantly, cochlear microphonics (CMs), a measure of the OHC receptor potential, were found to be phase-shifted and asymmetrical in form in *Tecta*^{ΔENT/ΔENT} mice. This suggested that the hair bundles of OHCs were responding to fluid flow rather than displacement in the absence of an attached TM, and no longer sitting with ~50% of their mechano-electrical transducer (MET) channels open at rest (Legan *et al.* 2000). These observations also led to the suggestion that the TM normally serves to bias the OHC hair bundles by shifting their position towards the excitatory direction, such that they operate around the mid-point of the relationship between bundle displacement and the amplitude of the receptor potential.

Thus far, however, the properties of the MET channels, the basolateral potassium conductance and prestin-based electromotility in the hair cells from mice lacking a functional TM have not been described and compared with those in wild-type mice. Therefore, the cellular origins of the observed hearing loss in these mice remain uncertain. In this study we used mice homozygous for null mutations in *Tecta* and *Tectb* (referred to as *Tecta/Tectb*^{-/-} mice) that, like the *Tecta*^{ΔENT/ΔENT} mice, no longer have a TM in contact with the organ of Corti (Fig. 1B). OHC development is normal in the absence of a functional TM, and MET channels have a resting open probability of ~50% in the presence of an extracellular concentration of Ca²⁺ similar to that found in the cochlear endolymph *in vivo* (40 μM, referred to hereafter as endolymphatic-like Ca²⁺). This large open probability ensures the optimal activation of the prestin. Analysis of auditory function *in vivo* revealed that long-lasting adaptation of distortion product otoacoustic emissions (DPOAEs) is completely

absent in the *Tecta/Tectb*^{-/-} mice, suggesting that the MET current in OHCs fails to adapt in the absence of TM. Therefore, TM may be responsible for regulating the Ca²⁺ concentration at or near the MET channels, thereby allowing adaptation of hair-cell MET currents during prolonged low-level repetitive auditory stimulation.

Materials and methods

Ethics statement

In the UK, experiments were performed in accordance with Home Office regulations under the Animals (Scientific Procedures Act) 1986 (PPL_PCC8E5E93) and following approval by the Ethical Review Committees of the Universities of Sheffield (180626_Mar) and Sussex. In Germany, care and use of the animals and the experimental protocol were reviewed and approved by the University of Tübingen, Veterinary Care Unit and the Animal Care and Ethics Committee of the regional board of the Federal State Government of Baden-Württemberg, Germany (permission number AZ 35/9185.82-2 §8a Abs.1 dated 21.07.16), and followed the guidelines of EU Directive 2010/63/EU for animal experiments.

Generation of *Tecta/Tectb* double knockout mouse (*Tecta/Tectb*^{-/-})

A targeting vector, which was designed and constructed by Vector Biolabs (Eagleville PA, USA) for deleting *Tecta* and expressing a *Tectb*-IRES-*Egfp* minigene under the control of the endogenous *Tecta* promoter, was generated using a combination of PCR and conventional cloning techniques. The vector consisted of a 2832 bp left arm with the ATG start codon of the *Tecta* open reading frame (ORF) at the 3' end fused via a PmeI linker to the *Tectb* ORF, followed by an IRES, the *Egfp* ORF, an SV40 polyadenylation signal sequence, a neomycin resistance cassette flanked with loxP sites, a 4903 bp right arm from the *Tecta* gene beginning 314 bp 3' of exon 2 and a thymidine kinase cassette. The *Tecta* arms were prepared from a 129SvEvBrd genomic DNA clone as described previously (Legan *et al.* 2000). For the generation of transgenic mouse line *Tecta*^{tm6Gpr}, embryonic stem cells were transfected with I-CeuI linearized targeting vector and resistant colonies selected as described (Legan *et al.* 2000). Individual colonies were picked and screened by Southern blotting and correctly targeted clones identified. Transgenic mice were prepared by microinjection of mouse blastocysts and a chimeric male founder was crossed with a wild-type S129SvEv female. Offspring carrying the insertion were then crossed with a beta-actin Cre line to remove the floxed neomycin selection cassette and, once it

had been established that the selection cassette had been deleted, the offspring were characterized.

Initial characterization of the *Tecta*^{tm6Gpr} transgenic line showed that while *TECTA* protein cannot be detected in mice homozygous for this allele, *Tectb* is not expressed under control of the *Tecta* promoter as originally intended because the PmeI linker introduces a frame shift, placing the entire *Tectb* coding sequence out of frame with the *Tecta* start codon. EGFP is, however, still expressed from the IRES under the control of the *Tecta* promoter and the spatial-temporal pattern of EGFP expression in the developing cochlea is very similar to that previously described with *in situ* hybridization using anti-sense probes for *Tecta* (Rau *et al.* 1999). The *Tecta*^{tm6Gpr} mouse, a *Tecta* null mutant mouse expressing EGFP at the *Tecta* locus, was subsequently crossed with the *Tectb*^{tm1Gpr} null mutant mouse line to produce a *Tecta*^{tm6Gpr/tm6Gpr}, *Tectb*^{tm1Gpr/tm1Gpr} double-null mutant mouse line that is referred to in this paper as the *Tecta/Tectb*^{-/-} double knockout mouse. Mice were bred onto a C57BL6/N background for at least five generations and wild-type C57BL/6N mice were used as controls.

Genotyping for the *Tecta*^{tm6Gpr} allele was done by PCR with KAPA2G Hot Start DNA polymerase (Sigma-Aldrich, UK) using primers TectbMGGF1 (CTCCCTGATAACCTACACTTC) and MmTectaEX1R1 (GAGCATGCTGATCAAGAGCTGTAGG) to amplify a wild-type product of 351 bp, and primers TectbMGGF1 and TectbMGGR1 (AACACAAGGATGACATCTGC) to amplify a mutant product of 339 bp. When resolved on a 1.5% agarose gel in 1 × TBE buffer a single 351 bp band indicates a *Tecta*^{+/+} genotype, two bands of 351 bp and 339 bp indicates a *Tecta*^{+/tm6Gpr} genotype and a single 339 bp band indicates a *Tecta*^{tm6Gpr/tm6Gpr} genotype. Genotyping for the *Tectb*^{tm1Gpr} allele was done by PCR with Fast Start Taq DNA polymerase (Roche, UK) in the presence of uracil-DNA glycosylase (Roche) and nucleotide mixes containing dUTP using primers MbKOF2 (GATTCAAGTGGTAACTGAGCTTCC) and MbKOR1 (GGCCAGGTCGCGATTGTTCTGTATC) to amplify a wild-type product of 376 bp, and primers MbKOF2 and PGKR9 (TGCACGAGACTAGTGAGACGTGCTA) to amplify a mutant product of 550 bp. When resolved on a 1.5% agarose gel in 1 × TBE buffer a single 376 bp band indicates a *Tectb*^{+/+} genotype, two bands of 550 bp and 376 bp indicates a *Tectb*^{+/tm1Gpr} genotype and a single 550 bp band indicates a *Tectb*^{tm1Gpr/tm1Gpr} genotype.

Single-hair cell electrophysiology

Tissue preparation. Apical-coil OHCs from wild-type and *Tecta/Tectb*^{-/-} double knockout mice of either sex were studied in acutely dissected organs of Corti

from postnatal day 7 (P7) to P31, where the day of birth is P0. After killing the mice using a Home Office-approved Schedule 1 method (cervical dislocation), cochleae were rapidly dissected and kept in the following extracellular solution (in mM): 135 NaCl, 5.8 KCl, 1.3 CaCl₂, 0.9 MgCl₂, 0.7 NaH₂PO₄, 5.6 D-glucose, 10 Hepes-NaOH, 2 sodium pyruvate. Eagle's minimum essential medium amino acid solution (X50, without L-Glutamine) and vitamin solution (X100) were added from concentrates (ThermoFisher Scientific, UK); pH was adjusted to 7.5, ~308 mOsmol kg⁻¹. Dissected cochleae were transferred to a microscope chamber, immobilized using a nylon mesh fixed to a stainless steel ring (Marcotti *et al.* 2003) and continuously perfused with the above extracellular solution. The sensory epithelia were viewed using an upright microscope (Olympus, Japan; Leica, Germany) with Nomarski differential interference contrast optics (X60 or X63 water immersion objectives and X10 or X15 eyepieces). All recordings were performed at room temperature (~22°C) unless otherwise stated.

Whole-cell patch clamp. Voltage and current recordings were performed using an Optopatch amplifier (Cairn Research Ltd, UK). Patch pipettes, with resistances of 2–3 MΩ, were pulled from soda glass capillaries and the shank of the electrode was coated with surf wax (Mr Zoggs Sex Wax, CA, USA). Basolateral currents were measured using the following intracellular solution (in mM): 131 KCl, 3 MgCl₂, 1 EGTA-KOH, 5 Na₂ATP, 5 Hepes-KOH, 10 sodium phosphocreatine (pH 7.3). For MET recordings, the intracellular solution contained (in mM): 106 L-glutamic acid, 20 CsCl, 10 Na₂phosphocreatine, 3 MgCl₂, 1 EGTA-CsOH, 5 Na₂ATP, 5 HEPES and 0.3 GTP (adjusted to pH 7.28 with 1 M CsOH; 294 mOsmol kg⁻¹). An L-glutamic acid-based intracellular solution was used as it preserves cellular ultrastructure and improves the stability of recordings (Kay, 1992). A similar solution has been used extensively for investigating the biophysical properties of mammalian cochlear hair cells (e.g. Corns *et al.* 2018; 2020; Jeng *et al.* 2020a,b). Data acquisition was performed using pClamp software (Molecular Devices, USA) using a Digidata 1440A. Data were lowpass filtered at 5 kHz (8-pole Bessel). Offline data analysis was performed using Origin 2019 software (OriginLab, USA). Membrane potentials were corrected for the residual series resistance (R_s) after compensation, and liquid junction potential (K⁺- and Cs⁺-based intracellular solution: -4 mV and -11 mV measured between electrode and bath solution, respectively). For some experiments, a gravity-fed local perfusion system was used to apply solutions with different extracellular Ca²⁺ concentrations (500 μM Ca²⁺ and endolymphatic-like 40 μM Ca²⁺) either alone or with 200 μM of the MET

channel blocker dihydrostreptomycin (DHS, Sigma, UK) (Marcotti *et al.* 2005).

Hair bundle stimulation. MET currents were elicited using a fluid jet from a pipette driven by a 25 mm diameter piezoelectric disc (Kros *et al.* 1992; Corns *et al.* 2014; 2018). The fluid-jet pipette tip had a diameter of 8–10 μm and was positioned at about 8 μm from the hair bundles to elicit a maximal MET current. Mechanical stimuli were applied as steps or 50 Hz sinusoids.

Electromotile response. Electromotility was estimated in OHCs at room temperature (~22°C) by applying a depolarizing voltage step from the holding potential of -64 mV to +56 mV and recorded using a CCD camera (Thorlabs DCU224M). The camera was attached to a microscope (Olympus), equipped with a X60 water immersion objective (Olympus LUMPlanFL N). The acquired images were stack-sliced along a vertical axis of each OHC and the contraction was measured on the image stack as length change of the cell. All images were analysed in ImageJ and the measurements were calibrated using a stage graticule (10 μm = 130 pixels).

Non-linear membrane capacitance. Nonlinear (voltage-dependent) capacitance was measured from P18 and P24 OHCs using whole-cell patch-clamp recordings. In order to block most of the ion channels in hair cells, the intracellular solution in the pipette contained (in mM): 125 CsCl, 3 MgCl₂, 1 EGTA-CsOH, 5 Na₂ATP, 5 Hepes-CsOH, 5 tetraethylammonium (TEA), 5 4-aminopyridine (4-AP) (pH was adjusted with CsOH to 7.28; 290 mOsmol kg⁻¹). Real-time changes in non-linear membrane capacitance (C_{N-L}) were investigated using the capacitance tracking-mode of the Optopatch amplifier (Cairn Research Ltd, UK) during the application of a 4 kHz sine wave of 13 mV RMS. From the holding potential of -84 mV, hair cells were subjected to a voltage ramp from -154 mV to +96 mV over 2 s. The capacitance signal from the Optopatch was lowpass filtered at 250 Hz and sampled at 5 kHz.

Immunofluorescence microscopy

Inner ears from wild-type and *Tecta/Tectb*^{-/-} mice ($n = 4$ for each experiment) were removed by dissection and fixed with 4% paraformaldehyde in phosphate-buffered saline (PBS, pH 7.4) for 20 min at room temperature. Cochleae were microdissected, rinsed three times for 10 min in PBS, and incubated for 1 h at room temperature in PBS supplemented with 5% horse serum (HS) and 0.5% Triton X-100. The samples were then incubated overnight at 37°C with the primary antibody in PBS supplemented with 1% HS. Primary antibodies were:

mouse anti-myosin 7a (1:1000, Developmental Studies Hybridoma Bank, #138-1C), rabbit anti-myosin 7a (1:200, Proteus Biosciences, #25-6790), rabbit anti-prestin (1:5000, kindly provided by Robert Fettiplace), rabbit anti-SK2 (1:500, Sigma-Aldrich, P0483) and goat anti-choline acetyltransferase (ChAT, 1:500, Millipore, AB144P). All primary antibodies were labelled with species-appropriate Alexa Fluor secondary antibody for 1 h at 37°C. Samples were then mounted in VECTASHIELD. The z-stack images were captured with a Nikon A1 confocal microscope equipped with Nikon CFI Plan Apo 60X Oil objective in the Light Microscope Facility at the University of Sheffield. Image stacks were processed with Fiji Image Analysis software (ImageJ, NIH and LOCI Laboratory of Optical and Computational Instrumentation, USA).

Toluidine blue staining

After glutaraldehyde fixation, cochleae were washed three times in 0.1 M sodium cacodylate buffer pH 7.2 and post-fixed in 1% osmium tetroxide in 0.1 M sodium cacodylate buffer for 3 h at room temperature. Samples were then washed three times in sodium cacodylate buffer and decalcified in 0.5 M EDTA pH 8.0 containing 0.1% glutaraldehyde for 3 days at 4°C. Samples were then washed briefly in water, dehydrated through an ascending ethanol series, equilibrated in propylene oxide and embedded in epoxy resin (TAAB 812). Blocks were cured at 60°C for 24 h and trimmed with a glass knife after which semi-thin 1 micron sections were cut on a Reichert Ultracut E ultramicrotome using a histo-grade Diatome diamond knife. Sections were dried onto glass slides and stained briefly with Toluidine blue before viewing on a Zeiss Axioplan 2 wide-field microscope. Images were captured using a Jenoptik ProgRes C3 CCD camera.

Scanning electron microscopy (SEM)

Cochleae were fixed by perfusing the cochlea with 2.5% glutaraldehyde in 0.1 M sodium cacodylate buffer (pH 7.2), and immersed in the same fixative overnight. Cochleae were then washed three times in 0.1 M sodium cacodylate buffer pH 7.2 and decalcified in 0.5 M EDTA pH 8.0 for 2–3 days at 4°C. Pieces of organ of Corti were then dissected in 0.1 M sodium cacodylate following the method described previously for cochlear wholemounts (Legan *et al.* 2014). Samples were then post-fixed in 1% osmium tetroxide for 3 h at room temperature, washed in cacodylate buffer and dehydrated through a series of ascending concentrations of ethanol. Following critical-point drying, samples were mounted on SEM stubs and sputter-coated with platinum before viewing in a Jeol JSM-6700F SEM operating at 5 kV.

In vivo hearing tests

Hearing tests. All recordings were performed on anaesthetized mice in a soundproof chamber (IAC, Niederkrüchten, Germany) as previously described (Knipper *et al.* 2000). In short, a multi-function IO-Card (PCI-6052E, National Instruments, USA) housed in a PC was used for stimulus generation and recording. Stimuli were delivered open field to the ear by loudspeakers either placed 3 cm lateral to the animal's pinna or as a closed field for otoacoustic measurements. Sound pressures were controlled with attenuators and amplifiers (Wulf Elektronik, Germany) and calibrated online prior to each measurement.

Anaesthesia. Mice were anaesthetized via intraperitoneal injection of 0.05 mg fentanyl dihydrogen citrate (Fentanyl-Ratiopharm 0.05 mg/ml, Ratiopharm, Ulm, Germany), 2 mg medetomidine hydrochloride (Sedator 5 mg/ml, Eurovet Animal Health B.V., Aulendorf, Germany), 5 mg midazolam hydrochloride (Dormicum 1 mg/ml, Hoffmann-La Roche AG, Grenzach-Wyhlen, Germany), 0.2 mg atropine sulfate (Atropin 0.5 mg/ml, Braun, Melsungen, Germany, to prevent circulation depression) mixed with water (Ampuwa, Fresenius KABI, Bad Homburg, Germany) to give a total of 10 ml injection volume per 1 kg body weight. After the injection, mice were immediately placed in a pre-warmed, darkened cage. The level of anaesthesia was monitored by heart rate, breathing rate and reflex tests for toe-pinch, eyelid and cornea, and additional doses of one third of the initial dose were subcutaneously supplemented if needed, usually every hour. Recovery from anaesthesia was obtained by subcutaneous injection of 1.2 mg Naloxon (Naloxon-hameln 2 mg/ml, Hameln Pharma plus GmbH, Hameln, Germany), 0.55 mg Flumazenil (Flumazenil-Kabi 0.1 mg/ml, Fresenius KABI) and 2.5 mg atipamezole hydrochloride (Antisedan 5 mg/ml, VETOQUINOL GmbH, Ravensburg, Germany) in water (Ampuwa) at 10 ml per 1 kg body weight.

Auditory brainstem responses (ABR). ABRs evoked by short-duration sound stimuli represent the summed neuronal activity along the auditory pathway (e.g. Möhrle *et al.* 2016). Briefly, ABRs were evoked by gated clicks, noise bursts, and pure tone stimuli of gradually increasing sound pressure in 5 dB steps at a repetition rate of 60/s. Clicks (100 μ s) and noise-burst stimuli (1 ms random phase frozen noise voltage signal) were rectangularly gated to produce sound signals emitted from the speaker dominated by a spectral peak at 7.9 kHz with a plateau of energy up to 35 kHz and a 30 dB roll-off from 35 to 65 kHz. Compared with the click stimulus, the noise-burst stimulus contained more energy at higher frequencies (>10 kHz). Pure tones were cosine square

(\cos^2) gated (3 ms duration, 1 ms rise/fall times) and presented for frequencies 2–45 kHz with two steps per octave. Stimuli were presented in open field by a loudspeaker (DT-911, Beyerdynamic, Heilbronn, Germany) and calibrated online with a microphone (B&K 4191, Brüel & Kjaer, Denmark) placed near the ear. The recorded signal was amplified (100 dB), filtered (0.2–5 kHz) and responses of alternating phase or polarity were summed to exclude the stimulus artefact and CMs. ABR thresholds were determined as the minimal sound pressure level able to induce a response that was identified by visual inspection of the averaged signal (Rüttiger *et al.* 2013; Möhrle *et al.* 2017).

Electrocochleographic recordings. We studied electrical potentials of cochlear OHCs and auditory nerve fibres by electrocochleography in living anaesthetized mice (wild-type: four males and five females; *Tecta/Tectb*^{-/-}: two males and 10 females; aged 2–6 months, average age 3.7 and 3.4 months for wild-type and *Tecta/Tectb*^{-/-} mice, respectively). Age and sex of the mice did not influence the electrical response. For these experiments, the surgery was done as previously described (Zampini *et al.* 2011). Briefly, mice were anaesthetized as described above (*Anaesthesia*) and 20–40 μ l of 2% Xylocain (AstraZeneca, Wedel, Germany) were applied subcutaneously at sites of surgical cuts. The bony auditory bulla was exposed by cutting the skin behind the ear and carefully traversing muscles, nerves and connective tissues avoiding displacing. A small hole (0.6 mm diameter) was drilled into the bulla and the round window niche of the cochlea visualized using an ultra-low speed drill rotation (down to two turns/s) in order to avoid any vibration-induced damage to the cochlea. A silver wire electrode insulated by varnish and silicone ending in a small silver bead was placed within the niche. The skin above the ear was closed and the mouse placed in the sound-attenuating booth in front of a loudspeaker for recording.

Compound action potential (CAP) threshold responses from the auditory nerves were determined by stimulation with short-tone pips (3 ms duration, 1 ms rise/fall times \cos^2 gated, 32–96 repetitions with stimulus interval 16 ms and alternating polarity) presented with 5 dB incremental steps from 0 to 110 (wild-type) or 40 to 120 dB SPL (*Tecta/Tectb*^{-/-}) between 2 and 64 kHz. Electrical potentials were amplified (80 dB) and filtered between 0.2 and 5 kHz before being sampled at 20 kHz A/D rate, averaged, and saved to file. Thresholds were determined from individual ears from averaged waveform responses as the lowest SPL resulting in a signal visually distinguishable from noise.

CAP amplitude growth. Electrical responses were recorded for 20 ms long 18 kHz pure tone stimuli

(0.2 ms \cos^2 gated) of 0–100 dB SPL (for wild-type mice) or 20–120 dB SPL (for *Tecta/Tectb*^{-/-} mice). Responses were amplified, filtered (DC, 50 kHz low pass), sampled at 100 kHz A/D rate, and averaged for 64 repetitions (ISI 50 ms). For CAP input–output analysis, the averaged waveform was digitally filtered (0.2–5 kHz, 6-pole, Hanning window, DC removed and phase corrected by twofold filtering with original and time-inverted time-amplitude series) and inspected for lowest and highest amplitude deflections (peaks) within a time window of 1 to 6 ms after stimulus onset. The peak-to-peak amplitude delineates the amount of synchronously active fibres within the auditory nerve as a CAP. The growth of the CAP is registered for each individual ear and the resulting growth functions from all ears averaged and presented as mean and standard deviation (SD).

Cochlear microphonic peak responses. CM signals, which are extracted from the electrocochleographic recordings, are mostly symmetric, fast potential changes from OHCs following the auditory stimulus pressure changes. Resulting average traces were analysed for their positive and negative peak of deflection within a 5 ms time window at 14–19 ms after stimulus onset (steady-state response). Resulting peak values were averaged for positive and negative peaks separately and displayed as a function of pressure (in Pascal).

Distortion product otoacoustic emissions. OHC function was assessed by the response strength and response threshold from the growth function and the distortion product audiogram of the cubic DPOAE in response to synchronous presentation of two stimulus tones (primaries 1 and 2). The cubic 2f₁-f₂ distortion product of the DPOAE for primary-tone frequency (f) f₂ = 1.24 × f₁ and primary-tone level (L) L₂ = L₁-10 dB were recorded in the soundproof chamber as previously described (Engel *et al.* 2006). Pairs of tones with frequencies between f₂ = 4 kHz and 32 kHz were presented directly into the ear canal by means of a metal coupler connected to two loudspeakers (DT-911, Beyerdynamic). The emission signals were recorded by a microphone (MK 231, Microtech, Gefell, Germany; Preamplifier Brüel & Kjaer 2670, Naerum, Denmark) connected to the coupler. Emission signals were recorded during sound presentation of 262 ms and averaged four times for each level and primary-tone frequency. For the distortion product audiogram, the 2f₁-f₂ distortion product amplitude was measured at constant L₂ of 50 dB SPL with pairs of primaries with frequencies between f₂ = 4 kHz and 32 kHz in four steps per octave. The growth function of the 2f₁-f₂ distortion product amplitude was measured for L₁ ranging from -10 to 65 dB SPL with pairs

of primary tones with frequencies between $f_2 = 4$ kHz and 32 kHz in half-octave steps. DPOAE thresholds were defined as the L1 level that could generate a $2f_1$ - f_2 signal reliably exceeding about 5 to 10 dB above noise level with noise level typically at -20 dB SPL.

DPOAE adaptation. During repeated loud sound stimulation, DPOAE can exhibit both short-lasting (fast) adaptation, which occurs within the 100 ms of the stimulus presentation (Kujawa & Liberman, 2001), and long-lasting adaptation that lasts more than minutes following the stimulus in rats (Zhao *et al.* 2018) and humans (Narahari *et al.* 2017). Fast DPOAE adaptation is believed to be mediated by cholinergic medial olivocochlear (MOC) efferent neurons (Robertson & Gummer 1985; Maison *et al.* 2003) and middle-ear muscle reflexes (MEMR: Horner, 1986). In order to elicit DPOAE adaptation in the ipsilateral ear, we repetitively exposed the ear to the two stimulus tones (primaries) with the frequencies $f_2 = 11.3$ kHz and $f_1 = 9.11$ kHz and with $L_1 = 60$ dB SPL and $L_2 = 50$ dB SPL for primaries 1 and 2, respectively (Wolter *et al.* 2018). Primaries were switched on synchronously, maintained for 100 ms and presented 384 times with 350 ms recording intervals. Onset and offset were \cos^2 gated with a 2 ms ramp. The aim of our work was to investigate the intrinsic activity of OHCs (by means of DPOAE), while avoiding the high stimulus levels that would activate the MOC and/or MEMR or induce adaptation effects by sound conditioning (for rabbits at *ca* 85 dB SPL: Luebke *et al.* 2015). Therefore, we first determined the DPOAE I/O growth function for $f_2 = 11.3$ kHz and $L_1 = -10$ to 65 dB SPL (non-adapted situation).

After inducing DPOAE adaptation, the DPOAE growth function for $f_2 = 11.3$ kHz was measured again. A change in the form of the $f_2 = 11.3$ kHz DPOAE growth function indicates whether DPOAE responses had adapted to the louder stimulus.

Data handling and presentation. Stimulus presentation, potential recording and filing was done by custom-made computer programs based on LabWindows-CVI (National Instruments) cards and libraries (CAP.exe, University of Tübingen). For single-sweep and averaged responses, data were filtered and processed by custom-made analysis computer programs (SingleSWEEP.exe and PEAK.exe, University of Tübingen). Results were exported to text files, arranged and visualized with Microsoft Excel.

Statistical analysis

For *in vitro* recordings, statistical comparisons of means were made by Student's two-tailed *t* test or, for multiple comparisons, using one-way ANOVA. Mean values are

quoted \pm SD, where $P < 0.05$ indicates statistical significance.

For *in vivo* recordings, data were compared for statistical difference by means of 2-way ANOVA (Graphpad Prism, San Diego, USA) and *post hoc* testing, with alpha-level corrected for multiple testing following the Bonferroni–Holms method or the Fisher's exact probability test for categorical frequency 2×2 contingency tables. For the frequency-dependent ABR and DPOAE data, and the waveform analysis, we used 2-way ANOVA and a *post hoc* Holm–Sidak's multiple comparison test. For click and noise burst stimulated ABRs, 2-sided Student's *t* test was used. In figures, statistical significance for pairwise comparisons are indicated by asterisks. n.s. denotes statistically non-significant results. Mean values are quoted \pm SD, where $P < 0.05$ indicates statistical significance.

Results

TM is detached from the organ of Corti in *Tecta/Tectb*^{-/-} mice

Toluidin blue-stained semi-thin sections and SEM were used to compare the structure of the organ of Corti and hair cell stereociliary bundles in wild-type (*Tecta/Tectb*^{+/+}) and *Tecta/Tectb* double knockout (*Tecta/Tectb*^{-/-}) mice (Fig. 1C). In wild-type mice the TM is attached medially to the spiral limbus and extends laterally, lying over the apical surface of the sensory hair cells (Fig. 1a). In the *Tecta/Tectb*^{-/-} mice, a residual TM is present but it is no longer associated with the luminal surface of the organ of Corti and is instead attached to Reissner's membrane (Fig. 1D). The structure, organisation and orientation of the hair bundles of the inner (not shown) and outer hair cells in the wild-type (Fig. 1E) and the *Tecta/Tectb*^{-/-} (Fig. 1F) mice are very similar. Material assumed to be derived from the TM is, however, often seen associated with the tips of the tallest row of stereocilia in the hair bundles of the OHCs in the wild-type (Fig. 1E, arrows), but not in the *Tecta/Tectb*^{-/-} mice (Fig. 1F). The structural phenotype of the cochlea in *Tecta/Tectb*^{-/-} mice is therefore very similar to that described previously for mice homozygous for a functional-null mutation (Δ ENT) in *Tecta* (*Tecta* ^{Δ ENT/ Δ ENT}; Legan *et al.* 2000).

Tecta/Tectb^{-/-} mice have a low- to mid-frequency hearing loss

The hearing in *Tecta/Tectb*^{-/-} mice was investigated using ABRs, a measure of the activity of the auditory neurons downstream of IHCs. Compared with wild-type mice (Figs. 2A–2E), aged-matched *Tecta/Tectb*^{-/-} mice had significantly higher ABR thresholds for click and

noise-burst stimuli (Figs. 2A, 2B), and for pure-tone stimuli ranging from 2 to 22.6 kHz (Fig. 2C). ABR thresholds were not detected in *Tecta/Tectb*^{-/-} mice for pure-tone stimulus frequencies below 4 kHz at the highest stimulus level tested (110 dB SPL). At higher pure-tone stimulus frequencies (32 and 45.3 kHz), the ABR thresholds of *Tecta/Tectb*^{-/-} mice were not significantly higher than those measured in wild-type mice (Fig. 2C). ABR thresholds are therefore raised in the most sensitive region of the hearing range in *Tecta/Tectb*^{-/-} mice, but are comparable to those of wild-type mice at high frequencies (Fig. 2C).

Extracellular recordings made from the round window of the cochlea in response to pure-tone stimuli reveal that the thresholds of the CAP are increased across the entire frequency range in the *Tecta/Tectb*^{-/-} mice (Fig. 2D). Thresholds are elevated by up to 60 dB in the mid-frequency range in the *Tecta/Tectb*^{-/-} mice and, above threshold, the CAP waveform amplitude grows slowly, relative to that in wild-type mice (Fig. 2E). These findings are in accordance with those from the *Tecta*^{DENT/DENT} mouse and confirm that the reduced ABR sensitivity of *Tecta/Tectb*^{-/-} mice occurs primarily at the level of the organ of Corti.

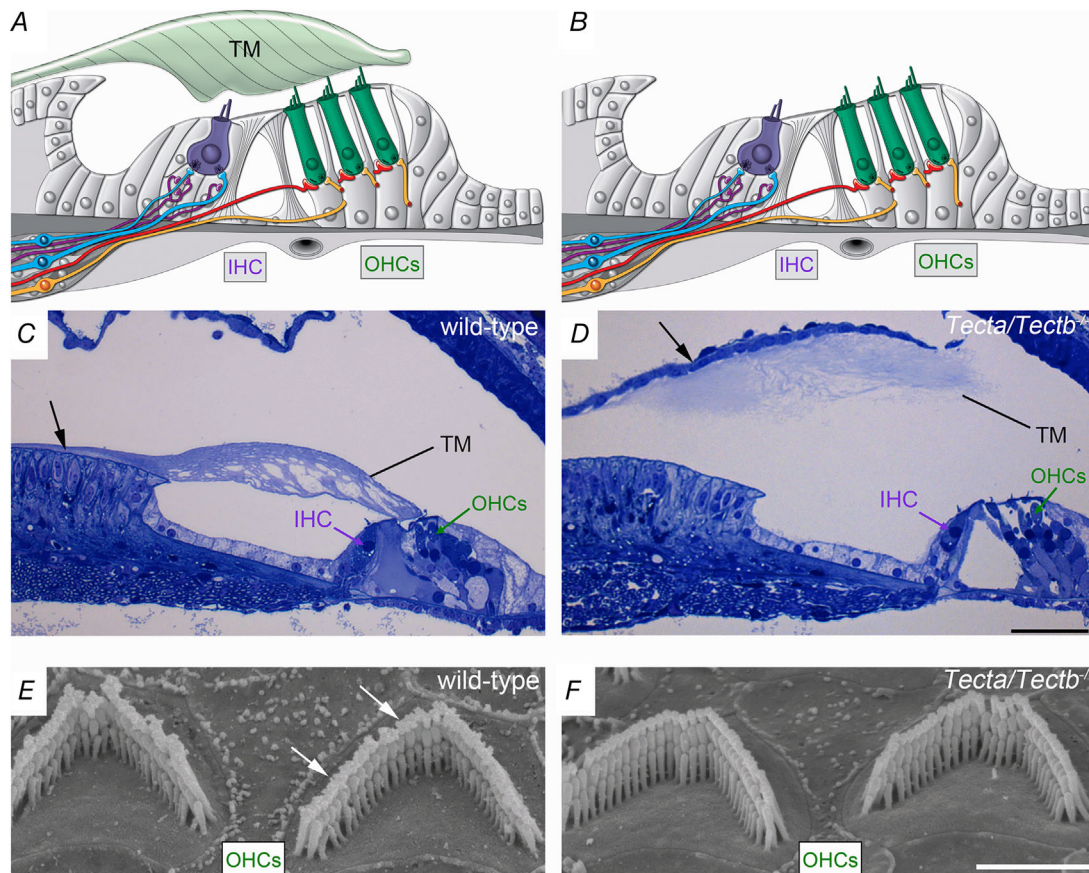


Figure 1. Tectorial membrane is detached in *Tecta/Tectb*^{-/-} mice

A and B, diagrams illustrating cross-sections of the mature organ of Corti in wild-type (A) and *Tecta*^{-/-} (B) mice (Legan *et al.* 2000). Abbreviations: TM: tectorial membrane, OHCs: outer hair cells, IHC: inner hair cell. Red and orange lines indicate the medial efferent and type II afferent fibres, respectively, making contacts with the OHCs. Blue lines indicate the type I afferent fibres making contacts with the IHCs. Violet lines indicate the lateral efferent fibres making contact with the type I afferent terminals. Cells depicted in grey represent the non-sensory cells within the organ of Corti. Note that the TM is in intimate contact with the tips of the tallest-row of stereocilia of the OHCs of wild-type (A) but not in *Tecta*^{-/-} (B) mice. C and D, Toluidine blue-stained semi-thin plastic sections from the apical coil of the cochlea of P21 wild-type and double knockout (*Tecta/Tectb*^{-/-}) mice, respectively. The tectorial membrane (TM) is attached to the spiral limbus in the wild-type (C, arrow) but completely detached in the mutant (D, arrow). Scale bars: 50 μ m. E and F, scanning electron microscopy images of the stereociliary bundle of mid-apical OHCs from P40 wild-type (E) and *Tecta/Tectb*^{-/-} (F) mice. Additional material is often associated with the tips of the taller row of stereocilia in the wild-type (arrows, E) but not with the *Tecta/Tectb*^{-/-} OHC bundles (F). Scale bars: 2 μ m.

Cochlear microphonics indicate symmetric OHC receptor potentials

CM potentials were recorded from the round window in response to an 18 kHz tone ranging in intensity from 50 to 100 dB SPL in the wild-type mice, and from 70 to 120 dB SPL in the *Tecta/Tectb*^{-/-} mice (Fig. 3A,B). Despite the variability in the phase of the response relative to the stimulus, the averaged waveform of CM in the *Tecta/Tectb*^{-/-} mice is symmetrical and similar to that of the wild-type. However, we noted a progressive phase shift with increasing stimulus level in the averaged response from the *Tecta/Tectb*^{-/-} mice (Fig. 3A,B), which was evident towards the later cycles within the first 0.5 ms

of the stimulus onset. This indicates that, in *Tecta/Tectb*^{-/-} mice, OHC hair bundles are likely to be fluid coupled to the stimulus. When the peak amplitudes of the CM waveforms measured at steady state 14–19 ms after stimulus onset are averaged across all ears of the same genotype and plotted as a function of pressure, the CM waveform was found to be symmetric in both genotypes (Fig. 3C,D). Furthermore, these data reveal that, the OHCs in both the wild-type and the *Tecta/Tectb*^{-/-} mice are operating around the steepest point on their input–output (transfer) functions. For examples of CM waveforms from individual animals, and the peak CM responses as function of pressure for all animals used to

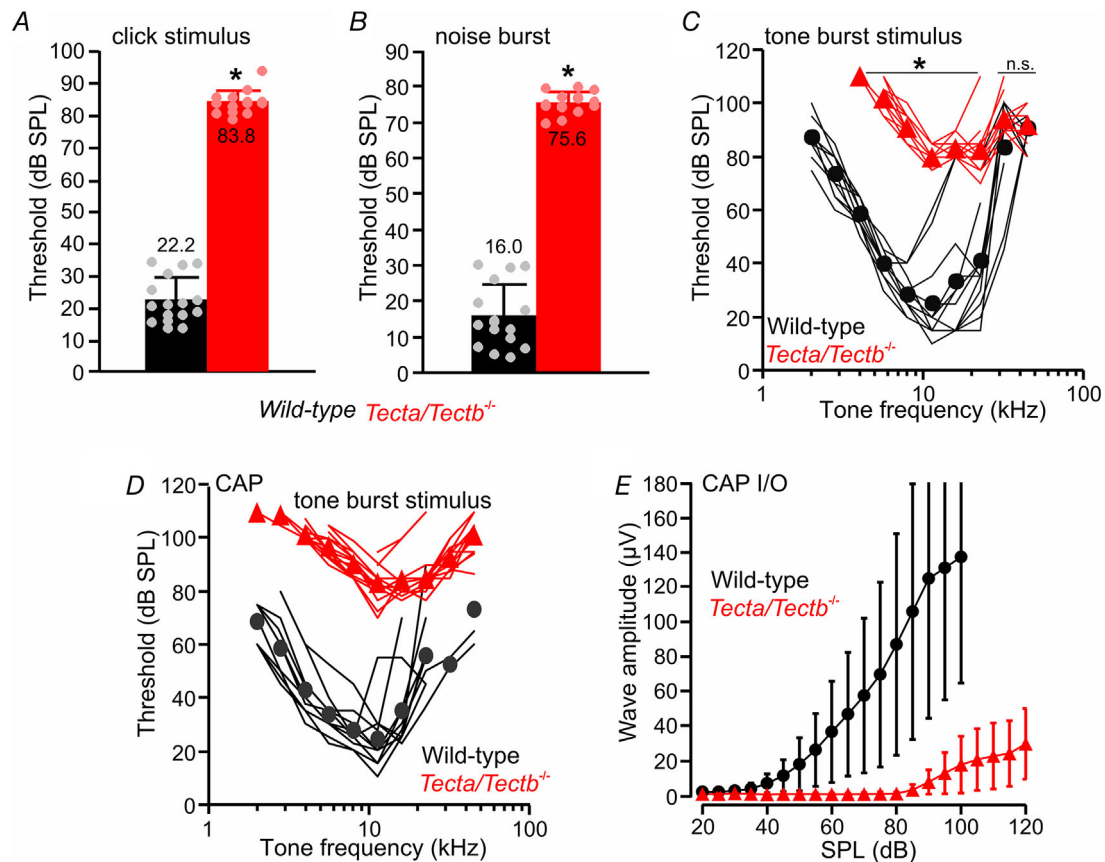


Figure 2. Auditory brainstem responses (ABRs) and compound action potentials (CAPs) in *Tecta/Tectb* mice

A and B, ABR thresholds evoked with a broadband click stimulus (A) and a noise-burst stimulus (B) from wild-type (8 mice, 16 ears) and *Tecta/Tectb*^{-/-} (8 mice, 15 ears) mice. Thresholds from single ear measurements are shown as dots superimposed on the average bar graph data. * $P < 0.0001$ in both A and B (2-sided Student's *t* test). C, ABR thresholds for a series of frequency-specific pure-tone stimuli from wild-type (8 mice, 12 ears) and *Tecta/Tectb*^{-/-} (8 mice, 15 ears) mice. Note that ABR thresholds increase across most of the frequency hearing range ($P < 0.0001$, two-way ANOVA; for Sidak's *post hoc* test see *Statistical Summary*). For two of the ears tested in the *Tecta/Tectb*^{-/-} mice, at 32–45 kHz ABR threshold could not be detected even with the highest stimulus levels. D, average CAP thresholds for frequency-specific pure-tone stimuli from wild-type and *Tecta/Tectb*^{-/-} mice ($P < 0.0001$, 2.8–45.2 kHz range, two-way ANOVA; for Sidak's *post hoc* test see *Statistical Summary*). E, growth of CAP responses across stimulus levels in wild-type and *Tecta/Tectb*^{-/-} mice. In *Tecta/Tectb*^{-/-} mice, CAP I/O function for 18 kHz stimuli above threshold was significantly different compared to that recorded in wild-type mice ($P < 0.0001$, two-way ANOVA; for Sidak's *post hoc* test see *Statistical Summary*). For the single data points in panel E, see Supplementary Data Set. Data are means \pm SD.

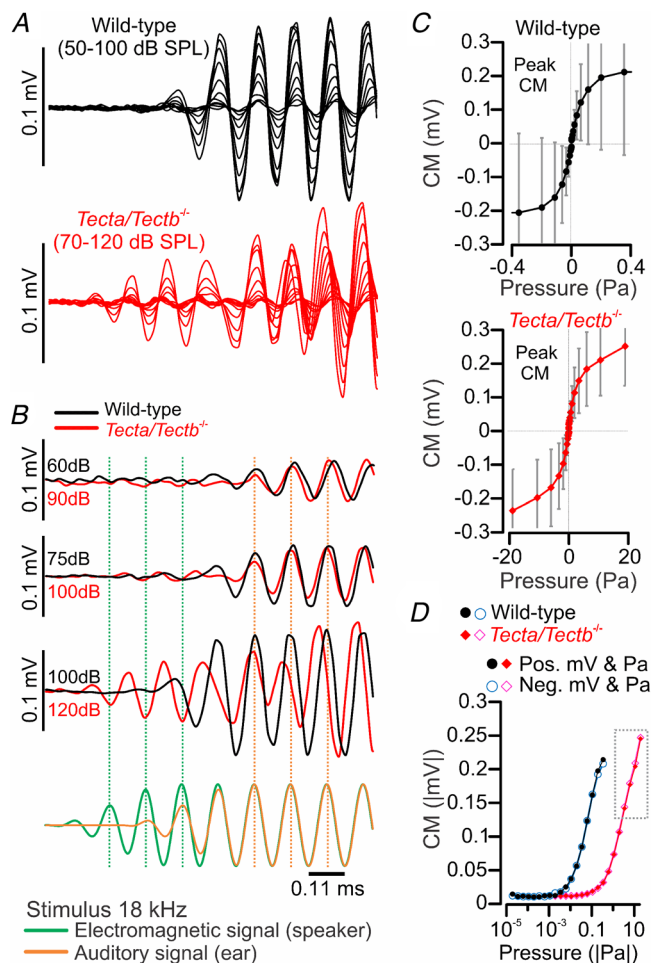


Figure 3. Cochlear microphonic signals in wild type and *Tecta/Tectb*^{-/-} mice

A, cochlear microphonic (CM) responses to 18 kHz pure-tone stimuli (gated with 0.2 ms \cos^2 ramp at onset) of increasing level averaged from 10 wild-type ears (top, black) and 18 *Tecta/Tectb*^{-/-} ears (bottom, red). Stimulus levels ranged from 50–100 dB SPL for the wild-type mice, and from 70–120 dB SPL for the *Tecta/Tectb*^{-/-} mice. Responses shown were recorded during the first 0.5 msec after onset of the stimulus. B, top three pairs of traces: averaged CM responses shown in panel A from wild-type (black) and *Tecta/Tectb*^{-/-} (red) mice are compared at stimulus levels eliciting potentials of comparable amplitude, at 60 and 90, 75 and 100, 100 and 120 dB SPL, respectively. For a comparison of CM responses from two individual animals see Supplemental Data Fig. 3B. Bottom: the green sinewave depicts the voltage driving the speaker that is delivering the stimulus and is located 3.8 cm from the pinna; the orange sinusoid shows the acoustic sound wave reaching the inner ear. At stimulus levels > 100 dB SPL, the driving voltage to the loudspeaker leads to significant electro-magnetic artifacts in the stimulus response that occur before the acoustic sound wave reaches the inner ear. C, peak CM response averaged from the individual ears of all wild-type (top, black) and all *Tecta/Tectb*^{-/-} (red, bottom) mice tested. The largest negative and largest positive peaks occurring within 15–20 ms after stimulus onset were averaged and plotted against sound pressure over the response range (wild-type mice: ± 0.4 Pa; *Tecta/Tectb*^{-/-} mice: ± 20 Pa). The negative and positive peaks of CM responses are symmetrical and not significantly different in both wild-type ($P = 0.5804$) and *Tecta/Tectb*^{-/-} ($P = 0.2744$) mice. Data are significantly different between wild-type and

Tecta/Tectb^{-/-} mice over the overlapping range of ± 0.4 Pa ($P < 0.0001$, two-way ANOVA). For the data from the individual animals that are averaged in panel C, see Fig. 3C in the Supplementary Data Set. D, data from panel C replotted with sound pressure on a log-scale. Peak negative and peak positive values of the CM response (solid symbols, Neg. mV and Pa values; open symbols, Pos. mV and Pa values) show considerable overlap highlighting the symmetry of the response. Dotted box indicates the values in the *Tecta/Tectb*^{-/-} affected by the electro-magnetic artifacts.

construct the averages shown in Fig. 3C, see Supplemental Data set.

DPOAE signals indicate lowered sensitivity but regular response strength in *Tecta/Tectb*^{-/-} mice

We measured DPOAEs to provide a better understanding of the functional consequences of the detached TM in *Tecta/Tectb*^{-/-} mice. In *Tecta/Tectb*^{-/-} mice, the amplitudes of the DPOAEs at 50 dB SPL stimulus level were greatly reduced (Fig. 4A) and the thresholds for evoking minimum DPOAE responses were increased to very high levels (Fig. 4B) compared with those in wild-type mice. DPOAE amplitude growth (I/O) function for stimuli with $f_2 = 11.3$ kHz (the frequency with the best DPOAE thresholds) revealed significantly lower values for DPOAE signal strength for stimulation levels between 20 and 55 dB SPL in *Tecta/Tectb*^{-/-} mice (Fig. 4C), although responses reached the levels of the wild-type mice above 55 dB SPL (Fig. 4C). As shown for the CM responses (Fig. 3), these results indicate that the stereociliary bundles of the OHCs are being stimulated by high-level sound simulation in the absence of an attached TM.

During repeated loud sound stimulation, DPOAE responses can exhibit both fast and long-lasting adaptation. Fast DPOAE adaptation, which can occur within 4 ms of the stimulus onset and can be elicited at levels of 50 dB SPL (Horner, 1986), is driven by neuronal feedback from the CNS via the MOC efferent system and the MEMRs. CNS feedback was not present in our recordings from either genotype (data not shown). In contrast to fast DPOAE adaptation, long-lasting adaptation can persist for minutes (Narahari *et al.* 2017; Zhao *et al.* 2018) and is not dependent on the feedback from the CNS. The characteristics of long-lasting DPOAE adaptation were investigated by exposing mice to 387 repetitions 100 ms long (inter-stimulus interval 350 ms) primary tones of 60 dB SPL over 2.25 min (135 s) (Figs. 4D–4F), a stimulus level that produced equally strong DPOAE responses in both genotypes (Fig. 4C). After presentation of the adapting stimulus for 2.25 min, the 2f₁-f₂ DPOAE response was found to be significantly reduced, compared with that obtained before exposure, in wild-type (Figs. 4D, 4F) but not in *Tecta/Tectb*^{-/-} mice (Figs. 4E, 4F).

Tecta/Tectb deletion does not affect hair-cell maturation

In order to ascertain whether the observed hearing defects (Fig. 2) are only due to the absence of the TM (Fig. 1), and not due to defects in hair-cell development, we investigated whether IHCs (Fig. 5) and OHCs (Figs. 6, 7) in *Tecta/Tectb*^{-/-} mice become mature, fully functional sensory receptors. Adult IHCs from wild-type mice express two characteristic K⁺ currents, a rapidly activating, large-conductance, Ca²⁺-activated K⁺

current *I*_{K,f}, and a negatively activating delayed-rectifier K⁺ current, *I*_{K,n} (Figs. 5A–5C) (Kros *et al.* 1998; Jeng *et al.* 2020c), with the latter carried by KCNQ4 channels (Kubisch *et al.* 1999). Both *I*_{K,f} and *I*_{K,n} in IHCs from *Tecta/Tectb*^{-/-} mice were not significantly different from those recorded in wild-type mice (Figs. 5D, 5E). Adult IHCs from *Tecta/Tectb*^{-/-} mice also exhibited voltage responses (Fig. 5F) and resting membrane potentials (Fig. 5G) that were similar to those in wild-type cells. Similar to IHCs, mature OHCs express *I*_{K,n} (Marcotti & Kros, 1999; Jeng *et al.* 2020a), which was present in

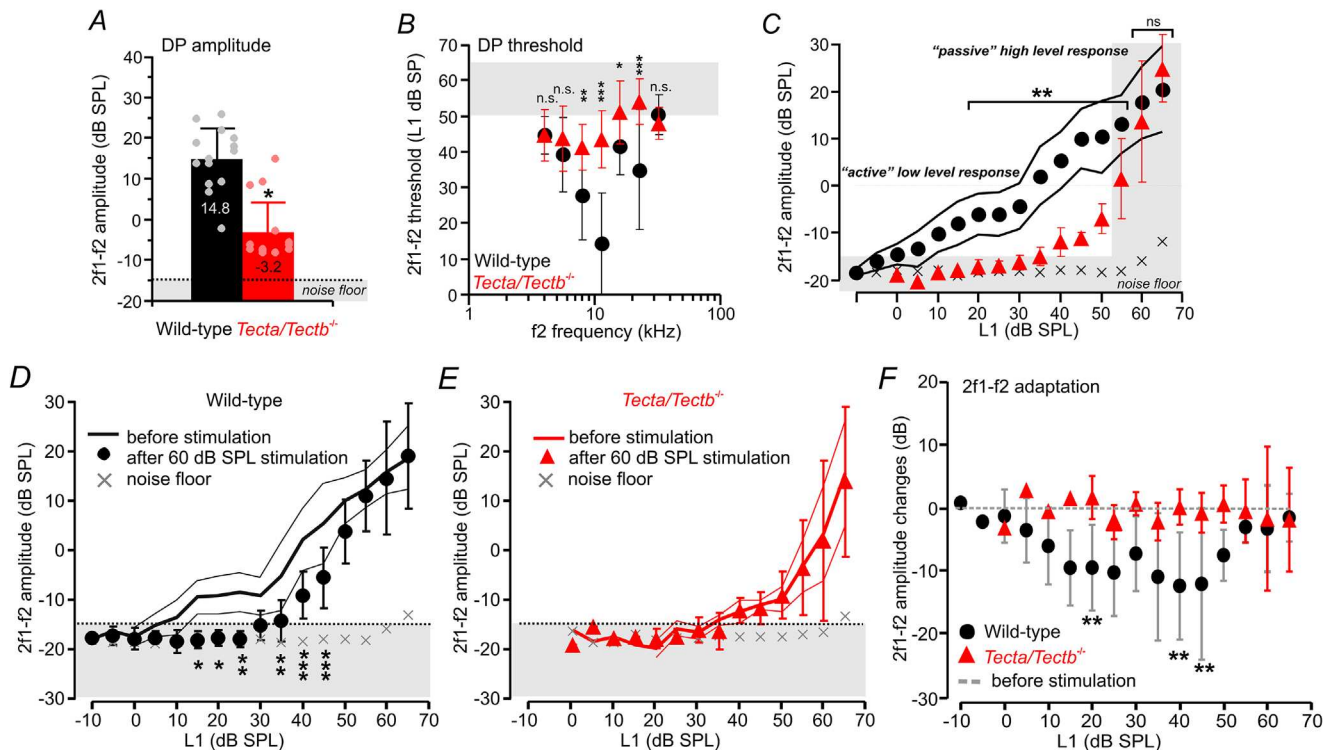


Figure 4. DPOAE responses adapt in wild-type but not in *Tecta/Tectb*^{-/-} mice

A, maximal amplitude of DPOAE signals from DP-grams measured over a range of primary-tone frequencies $f_2 = 4\text{--}32$ kHz at stimulation level $L_1 = 50$ dB SPL in both wild-type (black: 8 mice, 16 ears) and *Tecta/Tectb*^{-/-} (red: 8 mice, 15 ears) mice. Maximal DPOAE responses were present in both genotypes at frequencies $f_2 = 6.7\text{--}26.7$ kHz, but were found to be significantly reduced in *Tecta/Tectb*^{-/-} mice (*t* test, $*P < 0.0001$). **B**, DPOAE thresholds were significantly increased in *Tecta/Tectb*^{-/-} compared with wild-type mice for most of the frequency range used for hearing in mice ($P < 0.0001$, two-way ANOVA; for Sidak's *post hoc* test 'asterisks' see *Statistical Summary*). **C**, growth function of DPOAE signals with increasing stimulus level indicates loss of active amplification in the close-to-threshold range in the *Tecta/Tectb*^{-/-} mice, while high-level DPOAE signals reach amplitudes in a similar range as the wild-type mice ($P < 0.0001$, two-way ANOVA; for Sidak's *post hoc* test 'asterisks' see *Statistical Summary*). Lines: 95% confidence interval (CI_{95}). **D** and **E**, DPOAE growth function for $f_2 = 11.3$ kHz stimulated 2f1-f2 DPOAE signals using 60 dB SPL stimulation (384×100 ms long stimulus presentations, inter-stimulus interval 350 ms, within 2.25 min) in both wild-type (black: 6 mice, 11 ears) and *Tecta/Tectb*^{-/-} (red: 4 mice, 8 ears) mice. Continuous black and red lines show the mean signals before stimulation and the CI_{95} . Symbols show the signals directly after stimulation. Measured noise floor and critical threshold level of -15 dB SPL are illustrated by grey crosses and area, respectively. After stimulation, DPOAE signals were significantly reduced within 15–45 dB SPL stimulation in wild-type ($P = 0.0060$, two-way ANOVA, for Sidak's *post hoc* test see *Statistical Summary*) but not in *Tecta/Tectb*^{-/-} ($P = 0.7661$) mice. Data are means $\pm CI_{95}$ (before) and $\pm SD$ (after). **F**, comparison of 2f1-f2 adaptation in wild-type (black) and *Tecta/Tectb*^{-/-} (red) mice. The difference in adaptation is significantly dependent on stimulus level ($P = 0.0039$, 2-way RM-ANOVA, for Sidak's *post hoc* test 'asterisks' see *Statistical Summary*). The grey dashed line indicates non-adapting DPOAE signals (amplitude change = 0). For recordings from individual animal averages in panels B–F, see Supplementary Data Set. Data are means $\pm SD$.

both wild-type and *Tecta/Tectb*^{-/-} mice (Figs. 6A–6C). Current-clamp experiments also revealed normal voltage responses in OHCs from both genotypes (Figs. 6D, 6E) with a resting membrane potential that was not significantly different in wild-type and *Tecta/Tectb*^{-/-} mice (Fig. 6F). The membrane capacitance was also similar in OHCs from wild-type (11.8 ± 0.5 pF, $n = 4$) and *Tecta/Tectb*^{-/-} mice (12.2 ± 0.9 pF, $n = 5$, $P = 0.4706$, t test). Mature OHCs are also the primary target

of the cholinergic MOC neurons (Maison *et al.* 2003) which, by releasing the neurotransmitter acetylcholine (ACh) at their efferent terminals (Simmons *et al.* 1996), modulate OHC electromotility and therefore mechanical amplification in the adult cochlea (Guinan, 1996). Efferent inhibition of OHCs by ACh is caused by Ca^{2+} influx through $\alpha 9\alpha 10$ -nAChRs activating hyperpolarizing, small-conductance, Ca^{2+} -activated K^{+} channels (SK2 channels: Oliver *et al.* 2000; Katz *et al.* 2004; Marcotti

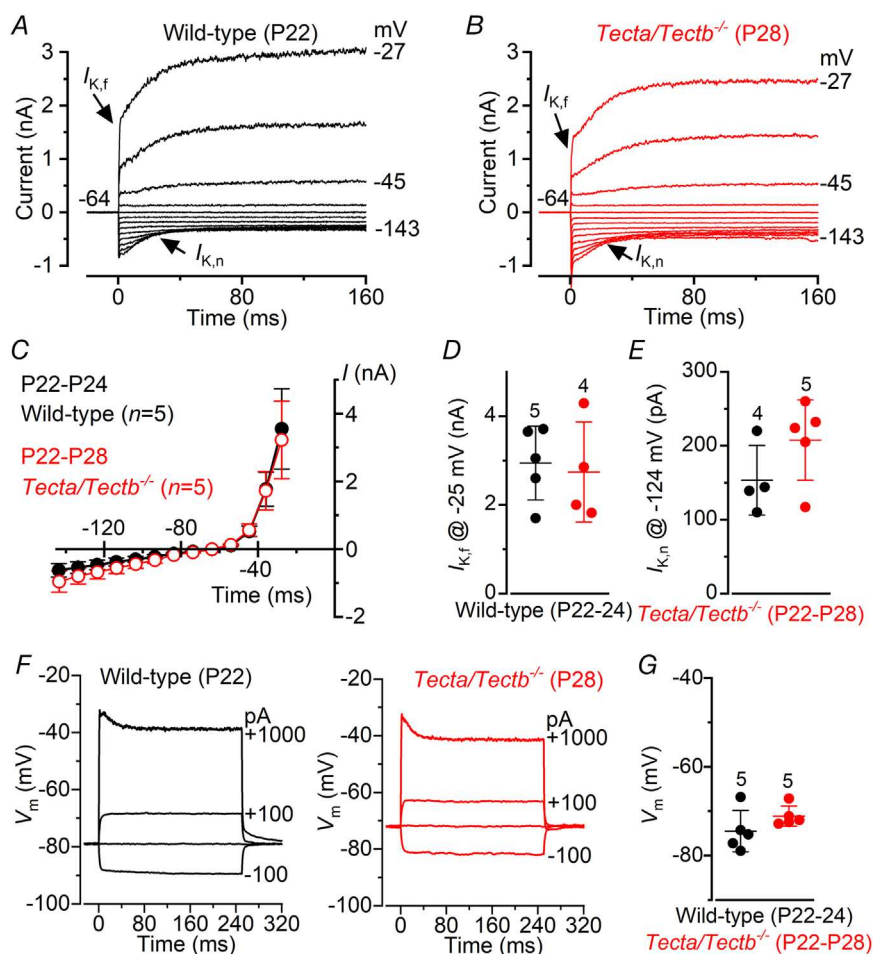


Figure 5. The basolateral membrane properties of adult IHCs are indistinguishable between wild-type and *Tecta/Tectb*^{-/-} mice

A and B, currents recorded from IHCs of wild-type (black) and *Tecta/Tectb*^{-/-} (red) post-hearing mice. Currents were elicited by using depolarizing voltage steps (10 mV increments) from the holding potential of -64 mV to the various test potentials shown by some of the traces. The arrow next to $I_{K,n}$ indicates the deactivating tail currents; while that next to $I_{K,f}$ indicates activation. C, steady-state current-voltage curves obtained from IHCs of wild-type (P22–P24) and *Tecta/Tectb*^{-/-} (P22–P28) mice. For recordings from individual hair cells in panel C, see Supplementary Data Set. D and E, size of the isolated $I_{K,f}$ (D), which was measured at -25 mV and at 1 ms from the onset of the voltage step, and $I_{K,n}$ (E) that was measured as the difference between the peak and steady-state deactivating tail current at -124 mV; for a similar analysis see: Marcotti *et al.* 2003. $I_{K,f}$ size: wild-type 2.9 ± 0.8 nA, $n = 5$; *Tecta/Tectb*^{-/-} 2.7 ± 1.1 nA, $n = 4$, $P = 0.7650$, t test. $I_{K,n}$ size: wild-type 153 ± 47 pA, $n = 4$; *Tecta/Tectb*^{-/-} 208 ± 54 pA, $n = 5$, $P = 0.1584$. F, voltage responses recorded from adult IHCs of wild-type and *Tecta/Tectb*^{-/-} mice elicited by applying hyperpolarizing and depolarizing current injections from their respective membrane potentials. G, average IHC resting membrane potential was not significantly different between wild-type (-74.5 ± 4.7 mV, $n = 5$) and *Tecta/Tectb*^{-/-} (-71.1 ± 2.3 mV, $n = 5$, $P = 0.1853$, t test). Single cell value recordings (closed symbols) are plotted behind the average values. Number of IHCs investigated is shown above the average data points. Values are means \pm SD. Recordings were performed at room temperature.

et al. 2004). Immunolabelling experiments confirmed that efferent cholinergic terminals, as visualized by ChAT immunoreactivity, and SK2 channels were both present in the OHCs of both wild-type and *Tecta/Tectb*^{-/-} mice (Fig. 6G).

As OHCs become functionally mature, from about P7 onwards, they acquire somatic motility (Marcotti & Kros, 1999; Abe *et al.* 2007), which is required for cochlear amplification and is driven by the motor protein prestin (SLC26A5; Zheng *et al.* 2000; Liberman *et al.* 2002). Voltage steps of 120 mV from the holding potential of -64 mV caused OHCs from both wild-type and *Tecta/Tectb*^{-/-} mice to shorten (Figs. 7A, 7B) by an amount (Fig. 7C) similar to that measured previously in other strains (Marcotti & Kros, 1999; Abe *et al.* 2007). This was further investigated using non-linear (voltage-dependent) capacitance changes (C_{N-L}), an electrical signature of electromotility in OHCs. We found that the maximum size of C_{N-L} in P18–P24 OHCs (Figs. 7D–7F) was comparable to that previously reported (e.g. Oliver & Fakler, 1999; Abe *et al.* 2007; Jeng *et al.* 2020a) and not significantly different in the two genotypes, consistent with the qualitative similar distribution of prestin observed in both genotypes (Fig. 7G).

These results show that OHCs and IHCs in *Tecta/Tectb*^{-/-} mice mature normally and acquire the

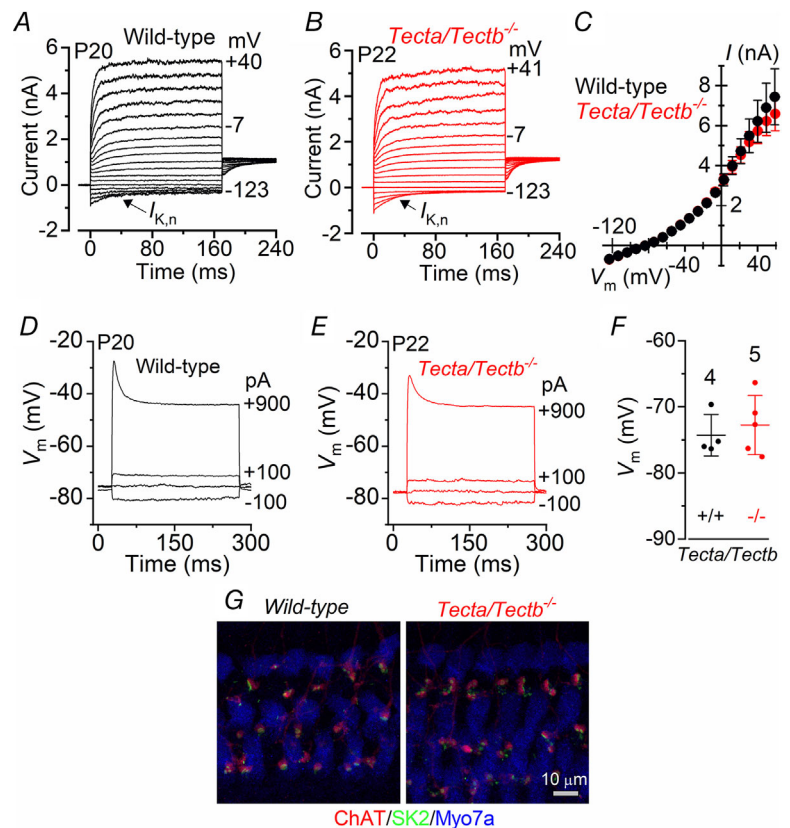
characteristic pattern of efferent innervation pattern, indicating that they do not require interactions with the TM to become fully functional receptors.

Mechanoelectrical transduction in mature OHCs from *Tecta/Tectb*^{-/-} mice

Considering that the basolateral membrane properties of OHCs are indistinguishable in wild-type and *Tecta/Tectb*^{-/-} mice, we sought to investigate whether the absence of DPOAE adaptation could be due to defects in the intrinsic characteristics of the MET apparatus. The structure of the hair bundles of P40 OHCs appeared comparable in wild-type and *Tecta/Tectb*^{-/-} mice (Fig. 1E,F), and we were able to record large MET currents in OHCs from both genotypes by displacing their hair bundles in the excitatory and inhibitory directions using a 50 Hz sinusoidal force stimulus from a piezo-driven fluid jet (Corns *et al.* 2014; 2016; 2018). At negative membrane potentials (-121 mV) in an extracellular solution containing 1.3 mM Ca²⁺, a large inward MET current could be elicited in P10 OHCs from both wild-type and *Tecta/Tectb*^{-/-} mice by deflecting the bundles towards the taller stereocilia (i.e. in the excitatory direction) (Fig. 8A). The resting current flowing through open MET channels in the absence of mechanical stimulation

Figure 6. Basolateral membrane currents in OHCs from *Tecta/Tectb*^{-/-} mice

A and B, currents recorded from a wild-type (P20) and a *Tecta/Tectb*^{-/-} (P22) OHC, respectively. Cells were held at -84 mV, and currents were elicited by voltage steps (10 mV increments). The holding currents are plotted as zero. C, average peak current-voltage relation obtained from four wild-type (P20–24) and six *Tecta/Tectb*^{-/-} (P22–23) OHCs. For recordings from individual hair cells in panel C, see Supplementary Data Set. D and E, voltage responses from mature OHCs of wild-type (D) and *Tecta/Tectb*^{-/-} mice (E), elicited using a series of hyperpolarizing or depolarizing current injections (shown next to the traces). F, resting membrane potential in wild-type (P20–24: -74.3 ± 3.1 mV, *n* = 4) and *Tecta/Tectb*^{-/-} (P22–27: -72.8 ± 4.5 mV, *n* = 5, *P* = 0.5790, *t* test) OHCs. G, maximum intensity projections of confocal z-stack images taken from mature apical-coil OHCs (P21) of wild-type and *Tecta/Tectb*^{-/-} mice. Immunostaining for SK2 channels (green) and ChAT (red), which is used to visualize the efferent olivocochlear innervation of OHCs; Myo7a (blue) was used as the hair cell marker. Similar staining was seen in four additional mice for each genotype. Scale bars: 10 μm.



was reduced when the bundles were moved towards the shorter stereocilia (i.e. in the inhibitory direction) in both wild-type and *Tecta/Tectb*^{-/-} OHCs (Fig. 8A, arrows). By stepping the membrane potential from -121 mV to +99 mV, the MET currents became outward during excitatory bundle stimulation, consistent with the non-selective permeability of the MET channels to cations. At positive potentials, which are near the Ca²⁺ equilibrium potential and strongly reduce Ca²⁺ entry via the MET channels, OHCs exhibited a larger resting MET current (Fig. 8A: arrowheads). This phenomenon is consistent with Ca²⁺ entry driving adaptation as previously demonstrated in hair cells from lower vertebrates

(Assad *et al.* 1989; Crawford *et al.* 1989; 1991) and mammals (Corns *et al.* 2014; 2016; Marcotti *et al.* 2016).

In previous studies it has only been possible to record MET currents *in vitro* from wild-type mouse OHCs prior to the onset of hearing at stages <P12, possibly because the transduction apparatus is damaged during physical removal of the TM. However, when using preparations from *Tecta/Tectb*^{-/-} mice in which the TM is no longer associated with the surface of the organ of Corti, we were able to record a large MET current in OHCs even after the onset of hearing (Fig. 8B: see also Jeng *et al.* 2020a). The maximal MET current at -121 mV in OHCs was plotted as a function of postnatal

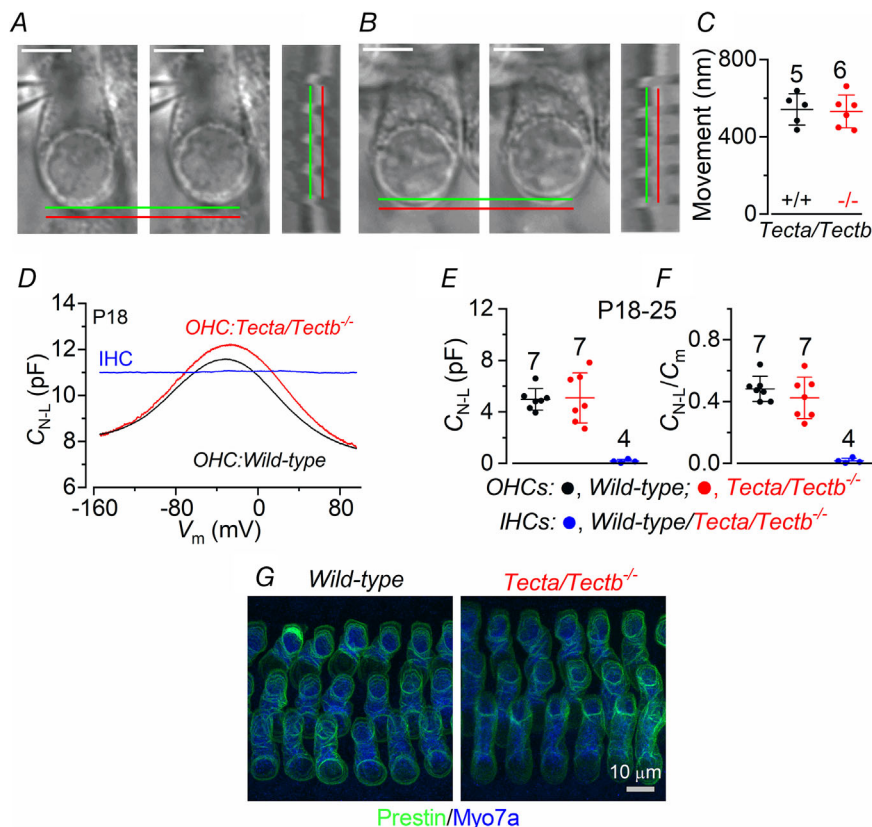


Figure 7. Prestin-driven electromotility in OHCs is normal in *Tecta/Tectb*^{-/-} mice

A and B, electromotile responses from a wild-type (P22) and a *Tecta/Tectb*^{-/-} (P19) OHC, respectively. The images of the OHCs in the left panels and right panels are obtained before and after, respectively, the application of a voltage step of 120 mV from the holding potential of -64 mV. Stacked images from repeating steps (right panels) are shown along a vertical axis of the basal-pole of the OHCs. Red and green lines indicate the position of the cell before and after the application of the voltage, respectively. Scale bar: 5 μ m. C, OHC contraction measured from wild-type (P22: 542 ± 81 nm, $n = 5$) and *Tecta/Tectb*^{-/-} (P19–27: 532 ± 85 nm, $n = 6$, $P = 0.8360$, t test) OHCs. D, voltage-dependent non-linear capacitance (C_{N-L}) recorded from P18 OHCs and IHCs by applying a voltage ramp from -154 mV to +96 mV. Note that C_{N-L} was present in the OHCs from both genotypes. E and F, average C_{N-L} was similar between wild-type and *Tecta/Tectb*^{-/-} apical-coil P18–P25 OHCs (E: wild-type 4.98 ± 0.84 pF, $n = 7$; *Tecta/Tectb*^{-/-} 5.07 ± 1.94 pF, $n = 7$, $P = 0.8979$, t test), even after normalization to the average OHC membrane capacitance C_m (F: wild-type 0.48 ± 0.08 , $n = 7$; *Tecta/Tectb*^{-/-} 0.42 ± 0.13 , $n = 7$, $P = 0.3465$, t test). Using the above protocol, IHCs only showed very small capacitance changes (183 ± 129 fF, $n = 4$, D–F: blue lines and dots), which were due to exocytosis of synaptic vesicles. Number of recordings are shown above the data points. Recordings are at room temperature. G, maximum intensity projections of confocal z-stacks taken from the apical cochlear region of wild-type and *Tecta/Tectb*^{-/-} mice at P21 stained with antibodies against prestin (green) and Myo7a (OHC marker: blue). Experiments were repeated from four mice of each genotype. Scale bars: 10 μ m.

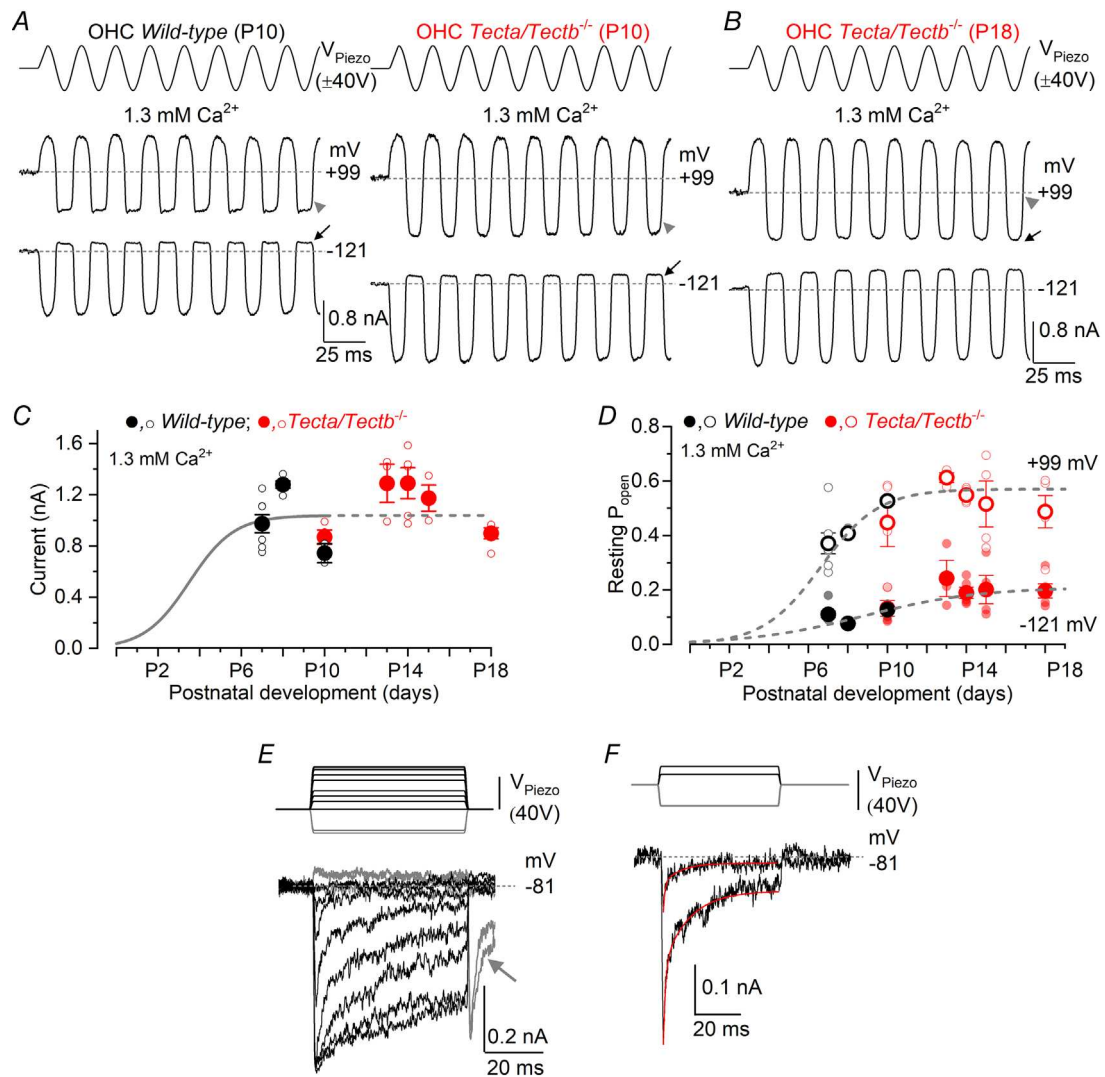


Figure 8. Mechanoelectrical transduction in *Tecta/Tectb*^{-/-} mice

A and B, saturating MET currents recorded from OHCs of wild-type (A, left, P10) and *Tecta/Tectb*^{-/-} (A, right, P10) pre-hearing mice, and post-hearing *Tecta/Tectb*^{-/-} mice (B, P18) by applying sinusoidal force stimuli of 50 Hz to the hair bundles at -121 mV and $+99$ mV. The driver voltage (V_{Piezo}) signal of ± 40 V to the fluid jet is shown above the traces (negative deflections of the driver voltage are inhibitory). Extracellular Ca^{2+} concentration was 1.3 mM. The arrows and arrowheads indicate the closure of the transducer currents (i.e. resting current) elicited during inhibitory bundle displacements at hyperpolarized and depolarized membrane potentials, respectively. Dashed lines indicate the holding current, which is the current at the holding membrane potential. C, maximal MET current recorded at different postnatal ages in wild-type (black) and *Tecta/Tectb*^{-/-} (red) OHCs. The number of OHCs tested from left to right: wild-type 7 (P7), 5 (P8), 2 (P10); *Tecta/Tectb*^{-/-} 4 (P10), 3 (P13), 5 (P14), 3 (P15), 5 (P18). The continuous grey line is a Boltzmann fit based on values from a large number of wild-type OHCs recorded over several years, showing the temporal acquisition of the MET current under our experimental conditions. The dashed line is extrapolated from the Boltzmann fit. D, resting open probability (P_{open}) of the MET channel plotted as a function of postnatal age in wild-type (black) and *Tecta/Tectb*^{-/-} (red) OHCs, and at the holding potential of -121 mV (solid circles) and $+99$ mV (open circles). The number of OHCs tested from left to right: wild-type 7 (P7), 5 (P8), 2 (P10); *Tecta/Tectb*^{-/-} 4 (P10), 3 (P13), 5 (P14), 4 (P15), 5 (P18). The dashed grey lines are a Boltzmann fit depicting the predicted changes in P_{open} with age, which was obtained by fitting the shown data extrapolated to 0 since, like most of the other features of the MET current, it develops postnatally (e.g. Lelli *et al.* 2009). E and F, MET currents recorded at -81 mV from a P18 *Tecta/Tectb*^{-/-} OHC by displacing the hair bundle with force-step stimuli (top panels). The MET current was elicited by 50 ms positive (excitatory) and negative (inhibitory) driver voltages to displace the stereociliary bundles (V_{Piezo}). The excitatory recordings in panel E were obtained using progressively larger driver voltages to show MET current adaptation more clearly. Upon termination of the inhibitory stimulus, the MET current showed evidence of rebound adaptation (E, arrow).

development in wild-type (P7–P10) and *Tecta/Tectb*^{-/-} (P10–P18) mice (Fig. 8C). The size of the MET current in OHCs of *Tecta/Tectb*^{-/-} mice after the onset of hearing (P13–P18: 1146 ± 257 pA, *n* = 16, at -121 mV) was not significantly different from that measured in wild-type mice just before the onset of hearing (P7–P10: 1051 ± 237 pA, *n* = 14, *P* = 0.300, *t* test). The MET current was also not significantly different between the two genotypes in pre-hearing OHCs (wild-type: P7–P10, 1051 ± 237 pA, *n* = 14; *Tecta/Tectb*^{-/-}: P10: 870 ± 113 pA, *n* = 4, *P* = 0.165, *t* test).

Despite the similar MET current size, the open probability of MET channels at rest in 1.3 mM Ca²⁺ was significantly larger in OHCs from mature mice (*Tecta/Tectb*^{-/-} P13–P18: 0.204 ± 0.074 at -121 mV; 0.535 ± 0.109 at +99 mV, *n* = 17) than that measured in cells of pre-hearing mice (wild-type P7–P10: 0.101 ± 0.030 at -121 mV, *n* = 14, *P* < 0.0001; 0.407 ± 0.088 at +99 mV, *P* = 0.0014) (Fig. 8D). However, the open probability of MET channels in P7–P10 wild-type OHCs (see above) was not significantly different from that measured in pre-hearing OHCs from *Tecta/Tectb*^{-/-} mice (P10: 0.133 ± 0.058 at -121 mV, *n* = 4, *P* = 0.523; 0.448 ± 0.176 at +99 mV, *P* = 0.165). These data show that while the maximum size of the MET current is already reaching mature-like values during the second postnatal week (pre-hearing), the Ca²⁺ sensitivity of the MET channel may only reach stable, possibly mature, characteristics after the onset of hearing. When OHC stereociliary bundles were deflected by excitatory fluid-jet force steps, from a holding potential of -81 mV, the MET current in mature OHCs from *Tecta/Tectb*^{-/-} mice declined or adapted over time (Fig. 8E). MET current adaptation to small bundle deflections was best fitted with a single exponential with a time constant of 0.73 ± 0.28 ms (*n* = 5) (Fig. 8F), a value not significantly different from the fast time constant previously measured in pre-hearing OHCs using a fluid jet (0.65 ± 0.31 ms, *n* = 14, *P* = 0.612; Corns *et al.* 2014). When inhibitory step deflections (negative driver voltages) were applied to the OHC hair bundle, the MET current shut off, revealing the small fraction of current flowing at rest. A transient rebound inward MET current was evident at the offset of the large inhibitory step (downward dip indicated by the arrow in Fig. 8E).

Calcium sensitivity of the MET channels in mature OHCs from *Tecta/Tectb*^{-/-} mice

A recent investigation has indicated that the MET channels located at the tip of the OHC stereocilia may, due to the TM acting as a source of Ca²⁺, be exposed to a Ca²⁺ concentration that is much higher (≥ ~500 μM; Strimbu *et al.* 2019) than that known to be present in end-

olymph (20–40 μM; Boshier & Warren, 1978; Ikeda *et al.* 1988; Salt *et al.* 1989; Wood *et al.* 2004). The effect of these two concentrations of extracellular Ca²⁺ on the OHC MET currents in mature *Tecta/Tectb*^{-/-} mice (P15–P21) is shown in Fig. 9A (40 μM Ca²⁺) and Fig. 9B (500 μM Ca²⁺). The size of the MET current at the membrane potential of -81 mV and in 40 μM Ca²⁺ (1.48 ± 0.25 nA, *n* = 9) was significantly larger than that measured in 500 μM Ca²⁺ (0.92 ± 0.29 nA, *n* = 8, *P* = 0.0003, Tukey's *post hoc* test, one-way ANOVA, Fig. 9C). The MET current size in 1.3 mM Ca²⁺ (1.09 ± 0.26 nA, *n* = 20) was significantly smaller than that measured in 40 μM Ca²⁺ (*P* = 0.0021), but comparable to the size in 500 μM Ca²⁺ (*P* = 0.2769, Tukey's *post hoc* test, one-way ANOVA). Extracellular Ca²⁺ is known to be a permeant blocker of the hair-cell MET channel (Ricci & Fettiplace, 1998; Marcotti *et al.* 2005), so the increased current amplitude in 40 μM Ca²⁺ is caused by the partial relief of this block. In agreement with previous observations from wild-type mice (Johnson *et al.* 2012; Corns *et al.* 2014), the presence of 40 μM Ca²⁺ increased the resting open probability (*P*_o) of the MET channels in the absence of mechanical stimulation (0.50 ± 0.13, *n* = 9, Fig. 9D), which was significantly larger than that measured in the presence of 500 μM (0.10 ± 0.05, *n* = 8, *P* < 0.0001, Fig. 9D) and 1.3 mM Ca²⁺ (0.19 ± 0.08, *n* = 20, *P* < 0.0001, Tukey's *post hoc* test, one-way ANOVA). This resting open probability (*P*_o) of the MET channel in 40 μM Ca²⁺ (0.50 ± 0.13, *n* = 9) was not significantly different from that measured at +99 mV (from Fig. 8D: 0.51 ± 0.12, *n* = 20, *P* = 0.7635, *t* test), a value that is near the Ca²⁺ equilibrium potential and strongly reduces Ca²⁺ entry into the MET channels (Assad *et al.* 1989; Crawford *et al.* 1989).

In order to test the physiological effects caused by the high Ca²⁺ concentration proposed to be present near the MET channel (~500 μM; Strimbu *et al.* 2019), relative to an endolymphatic concentration of 20–40 μM (see above), on mature OHCs, we performed current-clamp experiments while perfusing the stereociliary bundle with different Ca²⁺ concentrations (Figs. 9E–9H). In the presence of 1.3 mM Ca²⁺, which is the Ca²⁺ concentration present in the perilymph and also that normally used to perform *in vitro* recordings from hair cells, OHCs had a resting membrane potential (*V*_m) of -68.7 ± 4.2 mV (*n* = 5). When the hair bundles of OHCs were superfused with 500 μM Ca²⁺, the resting *V*_m did not change significantly (-66.5 ± 4.4 mV, *n* = 5, *P* = 0.8814, Tukey's *post hoc* test, one-way-ANOVA) compared with that measured in 1.3 mM Ca²⁺. The small depolarization in 500 μM Ca²⁺ was prevented when it was perfused together with the MET channel blocker dihydrostreptomycin (DHS) (Marcotti *et al.* 2005). In the presence of DHS the *V*_m of OHCs became even more hyperpolarized (-71.3 ± 3.6 mV, *n* = 5) than that recorded in 1.3 mM Ca²⁺, which was due to the block of the small resting MET current.

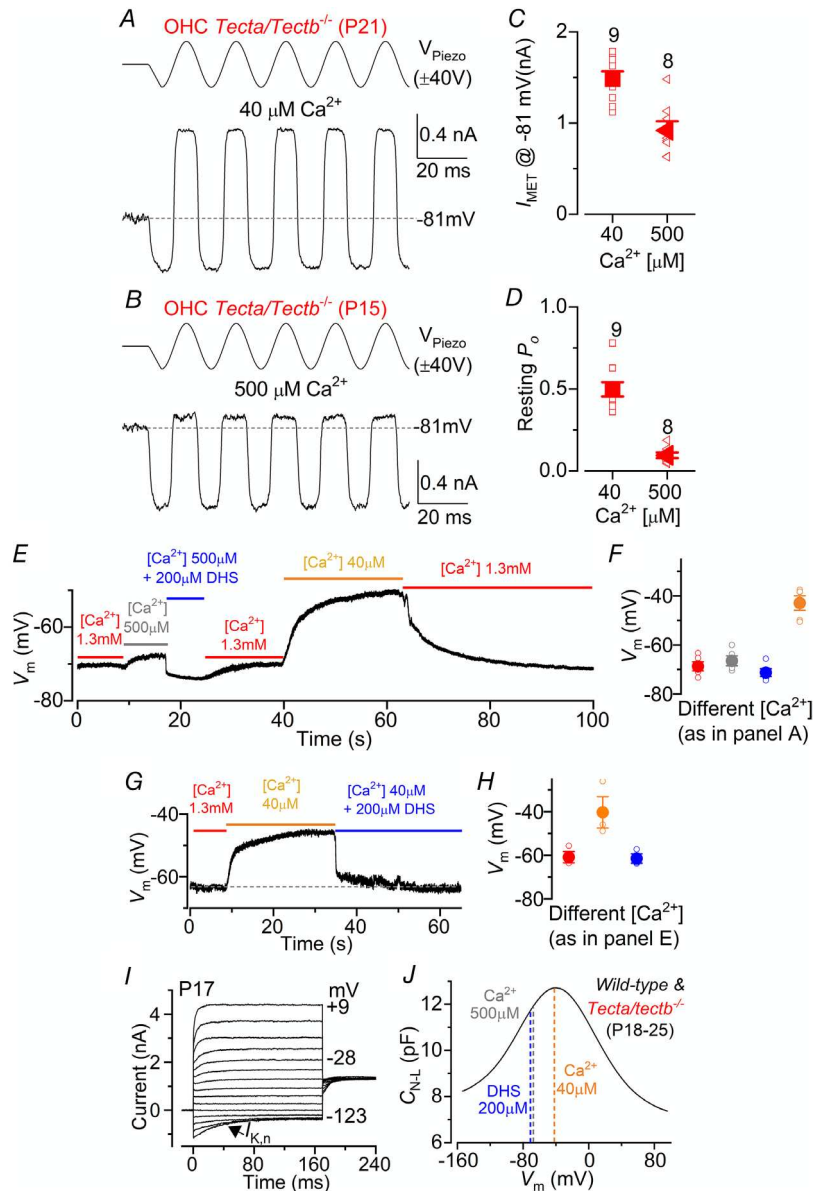


Figure 9. Effect of Ca^{2+} on the MET current and resting membrane potential of mature OHCs
 A and B, saturating mechanotransducer currents recorded from mature OHCs exposed to endolymphatic-like $40\ \mu\text{M}$ (A) and $500\ \mu\text{M}$ Ca^{2+} concentration (B). The driver voltage (DV) signal to the fluid jet is shown above the traces. Note that mechanotransducer current amplitude was larger and the fraction of current activated at rest (i.e. open probability of the MET channel: P_o) was increased in the presence of $40\ \mu\text{M}$ Ca^{2+} . C and D, maximum amplitude (C) and resting P_o (D) of the MET current in $40\ \mu\text{M}$ and $500\ \mu\text{M}$ Ca^{2+} concentrations. The resting open probability was calculated by dividing the MET current available at rest (the difference between the current level prior to the stimulus, indicated by the dashed line, and the current level on the negative phase of the stimulus when all channels were closed) by the maximum peak-to-peak MET current. E, voltage response under current clamp from a P17 *Tecta/Tectb*^{-/-} OHC. The stereociliary bundle of the OHC was superfused with different Ca^{2+} concentrations alone, or together with $200\ \mu\text{M}$ dihydrostreptomycin (DHS) in the presence of $500\ \mu\text{M}$ Ca^{2+} . F, average resting membrane potential (V_m) in different extracellular Ca^{2+} concentrations from five P17 OHCs. V_m in $40\ \mu\text{M}$ Ca^{2+} was significantly more depolarized compared with all other conditions ($P < 0.001$, Tukey's *post hoc* test, one-way ANOVA). G, voltage response as described in panel E, but during the perfusion of $40\ \mu\text{M}$ Ca^{2+} concentrations alone, or together with $200\ \mu\text{M}$ dihydrostreptomycin (DHS). H, average resting membrane potential (V_m) in different extracellular Ca^{2+} concentrations from three P15–P16 OHCs. V_m in $40\ \mu\text{M}$ Ca^{2+} was significantly more depolarized compared with all other conditions ($P = 0.0272$, one-way ANOVA). I, current responses from the same OHC shown in panel A, using the voltage protocol described for Fig. 6A. J, average non-linear capacitance traces from all 14 OHCs from Fig. 7D, but with the V_m from panel B.

However, OHCs showed a large depolarization in the presence of $40 \mu\text{M Ca}^{2+}$ ($-42.9 \pm 6.6 \text{ mV}$, $n = 5$), which was significantly greater than that observed in either 1.3 mM or $500 \mu\text{M Ca}^{2+}$ ($P < 0.0001$ for both comparisons, Tukey's *post hoc* test, one-way ANOVA, Figs. 9E, 9F) and is in agreement with previous observations made in mice (Johnson *et al.* 2011), and in rat OHCs with fully developed hearing ($\sim -40 \text{ mV}$: Oliver & Fakler, 1999; Mahendrasingam *et al.* 2010). We also showed that $200 \mu\text{M DHS}$ was also able to block the large membrane depolarization caused by $40 \mu\text{M Ca}^{2+}$ (Figs. 9G, 9H), indicating that the change V_m in it is driven by the opening of the MET channels ($P = 0.0272$, one-way ANOVA). Figure 9I shows the membrane currents recorded from the same OHC shown in Fig. 9E at the end of the experiment, which highlights the presence of viable OHCs. Since the resting V_m of OHCs is crucial to optimally activate prestin (Oliver & Fakler, 1999), we determined where the cells would be operating on the voltage-dependent non-linear capacitance curve (Fig. 7D) at the average V_m obtained using the different Ca^{2+} concentrations (Fig. 9F). We found that in the presence of $40 \mu\text{M Ca}^{2+}$ surrounding the stereociliary bundle, but not in the proposed higher $[\text{Ca}^{2+}]$ (Strimbu *et al.* 2019), the V_m of OHCs is sitting at the best activation voltage for prestin modulation (Fig. 9J).

Discussion

The results of this study show that detachment of the TM from the surface of the organ of Corti (Fig. 1) causes a significant elevation of ABR thresholds in *Tecta/Tectb*^{-/-} mice (up to $\sim 60 \text{ dB}$ in the 8–15 kHz frequency range). The possible contribution of dysfunctional hair cells to the hearing phenotype in *Tecta/Tectb*^{-/-} mice can be excluded as the TM is not required for the functional maturation of their biophysical properties (Figs. 5–7), including those of the MET apparatus (Fig. 8). The TM is, however, required to ensure that the primary stimulus (sound-induced basilar membrane motion) drives the hair bundles of the hair cells with high sensitivity especially at low-to-moderate sound pressure levels (Fig. 2). The results also demonstrate that, *in vitro*, the resting open probability of the MET channel in mature OHCs, a manifestation of the channel's Ca^{2+} -dependent adaptation characteristics, reaches values of $\sim 50\%$ in a concentration of Ca^{2+} similar to that in endolymph ($40 \mu\text{M}$). The large resulting resting MET current depolarizes mature OHCs close to the best level for activation of the motor protein prestin, thus providing optimal cochlear amplification (Fig. 9). *In vivo*, a large open probability of the MET channels was encountered irrespective of the presence or absence of a TM, indicating that the TM is unlikely to statically bias the resting position of the OHC stereociliary bundle (Fig. 3). Finally, long-lasting adaptation of DPOAEs following prolonged stimulation

depends on the presence of the TM (Fig. 4), indicating that the TM may contribute to regulating Ca^{2+} levels around the stereocilia and therefore MET channel adaptation *in vivo*.

Mechanoelectrical transduction in adult OHCs from *Tecta/Tectb*^{-/-} mice

An unexpected benefit of characterizing the biophysical properties of hair cells in the *Tecta/Tectb*^{-/-} mice was that MET current recordings could, for the first time, be investigated in mature OHCs *in vitro*. Genetic, as opposed to physical, removal of the TM from the hair bundles of the OHCs to which it is considered to be firmly attached (Kimura, 1966) therefore appears to prevent damage to the stereocilia and/or the MET channel complex. Using this novel experimental approach, we demonstrated that most of properties of the MET currents in mature OHCs of *Tecta/Tectb*^{-/-} mice are similar to those in wild-type OHCs prior to the onset of hearing at P12. As shown for rat (Kennedy *et al.* 2003) and mouse (Corns *et al.* 2014) OHCs, the size of the MET current reaches a mature-like level towards the end of the second post-natal week. The Ca^{2+} sensitivity of the MET channel, however, only acquires mature characteristics after the onset of hearing, with an average resting open probability of $\sim 50\%$ in concentrations of Ca^{2+} ($40 \mu\text{M}$) similar to those known to be present in endolymph ($20\text{--}40 \mu\text{M}$: Boshier & Warren, 1978; Ikeda *et al.* 1988; Salt *et al.* 1989; Wood *et al.* 2004). The latter finding suggests low Ca^{2+} around the hair bundle is sufficient to account for the symmetrical receptor potentials previously recorded from mature OHCs *in vivo* (Russell & Sellick 1983).

Function of the tectorial membrane in the mammalian cochlea

The fully mature TM-OHC configuration is reached over a period of 2–3 weeks during pre-hearing stages of development in mice (reviewed by Goodyear & Richardson, 2018). This time window is also associated with other major morphological and physiological changes in the cochlea (Pujol *et al.* 1998). Considering that the development of hair cells depends to a large extent on spontaneous electrical activity generated within the organ of Corti (IHCs: Johnson *et al.* 2013; Johnson *et al.* 2017; OHCs: Ceriani *et al.* 2019; Jeng *et al.* 2020c), it is perhaps not surprising that hair cells mature normally in the absence of an attached TM. Nonetheless, this information is required before drawing further conclusions about the origin of the elevated ABR thresholds. As the biophysical properties of hair cells were unaffected by the absence of an attached TM, and as the thresholds of the CAP and CM (readouts of the activity of the auditory afferent fibres and OHC receptor potential, respectively) recorded at the

round window were elevated in the *Tecta/Tectb*^{-/-} mouse, one can conclude that the TM is required to efficiently drive the deflection of the hair bundle. Amplification of the basilar membrane motion by the OHCs will therefore be reduced in the absence of a TM, as will the motion of the fluid in the sub-tectorial space that drives the displacement of the hair bundles of the IHCs. This, in turn, will reduce neurotransmitter release at the ribbon synapses of the IHCs and result in an increase in ABR and CAP thresholds.

A previous study performed on mice with a detached TM (*Tecta*^{ΔENT/ΔENT} mice; Legan *et al.* 2000) provided evidence for an asymmetry of the peak amplitude CM responses to positive and negative sound pressure levels, indicating only a small fraction of the MET channels were open at rest. This finding suggested that the TM statically biases the position of the hair bundles of the OHCs in wild-type mice in the excitatory direction, thereby allowing the cells to sit with 50% of their MET channels open and operate around the most sensitive (steepest) region of the input–output function (Legan *et al.* 2000). However, considering the narrow operating range of the OHC, estimated to be <200 nm for mouse OHCs (Géléoc *et al.* 1997; He *et al.* 2004; Corns *et al.* 2014; Fettiplace & Kim, 2014; Marcotti *et al.* 2016) it is hard to conceive how the TM can achieve such a precise spatial bias on the hair bundles. Furthermore, the symmetry of the CM waveforms in the wild-type and the *Tecta/Tectb*^{-/-} mice are very similar. The data therefore fail to provide evidence that the TM statically biases the operating point of the hair bundles of the OHCs, and indicates that the OHCs have 50% of MET channels open at rest irrespective of the presence or absence of a TM. Considering the morphological similarity of the cochlea in the *Tecta*^{ΔENT/ΔENT} (Legan *et al.* 2000) and the *Tecta/Tectb*^{-/-} mice, the discrepancy in the findings between the two mouse lines is unclear. Possible reasons could include differences in genetic background (mixed/variable C57BL/6J-S129SvEv; Legan *et al.* 2000; C57BL/6N; present study) or the averaging of data across a larger sample size. Furthermore, we found that DPOAE responses in *Tecta/Tectb*^{-/-} mice at L1 levels >40 dB SPL lack long-lasting adaptation, a process that adjusts the OHC response into the physiological range. This finding provides evidence that the TM is required for adaptation of the hair-cell MET channel, a process that is known to require Ca²⁺ (Assad *et al.* 1989; Crawford *et al.* 1991; Corns *et al.* 2014; Marcotti *et al.* 2016).

MET channel adaptation during repetitive sound stimulation may require the TM

Recently, it has been shown that the Ca²⁺ concentration within the TM of the guinea pig is likely to be much higher (≥500 μM depending on the cochlear region; Strimbu

et al. 2019; see also: Anniko & Wroblewski, 1980) than that found in the surrounding endolymph (20–40 μM; Bosher & Warren, 1978; Ikeda *et al.* 1988; Salt *et al.* 1989; Wood *et al.* 2004). Furthermore, very loud sounds, similar to those used to cause a temporary threshold shift, can deplete Ca²⁺ from the TM (Strimbu *et al.* 2019). These data have led to the suggestion that the TM may release Ca²⁺ and thus elevate the concentration in the vicinity of the MET channels to more than is required to sustain normal transduction and adaptation (Strimbu *et al.* 2019). However, the CM recordings made from the round window of *Tecta/Tectb*^{-/-} mice *in vivo* showed that the OHC receptor potential is symmetrical in shape (Fig. 3), which is only likely to occur in the presence of endolymphatic-like extracellular Ca²⁺ (Fig. 9: i.e. the open probability of the MET channel is ~50% in 40 μM Ca²⁺). In the presence of 500 μM Ca²⁺ surrounding the hair bundle, similar to that found in certain regions of the TM (Strimbu *et al.* 2019), the open probability of the MET channel drops to ~10%, a value that is inconsistent with the symmetrical CM responses. Additionally, in the presence of 40 μM Ca²⁺, the large MET current flowing into the OHCs depolarizes them to near -40 mV, a potential that reduces the membrane time constant and allows optimal activation of the motor protein prestin, both crucial for normal cochlear amplification. In contrast, the relatively hyperpolarized membrane potential found in the presence of 500 μM Ca²⁺ (~-65 mV) is sub-optimal and would compromise amplification (Fig. 9). It therefore seems likely that, either with or without the TM, the set point of the OHC receptor transfer function is determined principally and by the endolymphatic Ca²⁺ concentration. As adaptation of the DPOAEs following repetitive lower-level stimulation depends on the presence of the TM, our findings raise the possibility, as yet to be proven, that MET current adaptation *in vivo* may rely on the TM regulating the Ca²⁺ concentration near the MET channel. The TM may directly contribute to increase the Ca²⁺ concentration near the MET channels (Strimbu *et al.* 2019) and/or act as a 'diffusion barrier' for Ca²⁺ extruded by the stereocilia via the plasma membrane Ca²⁺-ATPase PMCA2, a protein that is highly expressed in OHCs but less so in IHCs (Chen *et al.* 2012; Fettiplace & Nam, 2019).

References

- Abe T, Kakehata S, Kitani R, Maruya S, Navaratnam D, Santos-Sacchi J & Shinkawa H (2007). Developmental expression of the outer hair cell motor prestin in the mouse. *J Membr Biol* **215**, 49–56.
- Anniko M & Wroblewski R (1980). Elemental composition of the mature inner ear. *Acta Otolaryngol* **90**, 425–430.
- Ashmore J (2018). Outer Hair Cells and Electromotility. *Cold Spring Harb Perspect Med* pii, a033522.

- Assad JA, Hacohen N & Corey DP (1989). Voltage dependence of adaptation and active bundle movement in bullfrog saccular hair cells. *Proc Natl Acad Sci USA* **86**, 2918–2922.
- Bosher SK & Warren RL (1978). Very low calcium content of cochlear endolymph, an extracellular fluid. *Nature* **273**, 377–378.
- Ceriani F, Hendry A, Jeng JY, Johnson SL, Stephani F, Olt J, Holley MC, Mammano F, Engel J, Kros CJ, Simmons DD & Marcotti W (2019). Coordinated calcium signalling in cochlear sensory and non-sensory cells refines afferent innervation of outer hair cells. *EMBO J* **38**, e99839.
- Cheatham MA, Zhou Y, Goodyear RJ, Dallos P & Richardson GP (2018). Spontaneous Otoacoustic Emissions in Tecta^{Y1870C/+} mice reflect changes in cochlear amplification and how it is controlled by the tectorial membrane. *eNeuro* **5**.
- Chen Q, Mahendrasingam S, Tickle JA, Hackney CM, Furness DN & Fettiplace R (2012). The development, distribution and density of the plasma membrane calcium ATPase 2 calcium pump in rat cochlear hair cells. *Eur J Neurosci* **36**, 2302–2310.
- Corns L F, S L Johnson C J Kros & Marcotti W (2014). Calcium entry into stereocilia drives adaptation of the mechano-electrical transducer current of mammalian cochlear hair cells. *Proc Natl Acad Sci USA* **111**, 14918–14923.
- Corns LF, Johnson SL, Kros CJ & Marcotti W (2016). Tmcl Point Mutation Affects Ca²⁺ Sensitivity and Block by Dihydrostreptomycin of the Mechano-electrical Transducer Current of Mouse Outer Hair Cells. *J Neurosci* **36**, 336–349.
- Corns LF, Johnson SL, Roberts T, Ranatunga KM, Hendry A, Ceriani F, Safieddine S, Steel KP, Forge A, Petit C, Furness DN, Kros CJ & Marcotti W (2018). Mechanotransduction is required for establishing and maintaining mature inner hair cells and regulating efferent innervation. *Nat Commun* **9**, 4015.
- Crawford AC, Evans MG & Fettiplace R (1989). Activation and adaptation of transducer currents in turtle hair cells. *J Physiol* **419**, 405–434.
- Crawford AC, Evans MG & Fettiplace R (1991). The actions of calcium on the mechano-electrical transducer current of turtle hair cells. *J Physiol* **434**, 369–398.
- Dallos P (1992). The active cochlea. *J Neurosci* **12**, 4575–4585.
- Engel J, Braig C, Rüttiger L, Kuhn S, Zimmermann U, Blin N, Sausbier M, Kalbacher H, Münkner S, Rohbock K, Ruth P, Winter H & Knipper M (2006). Two classes of outer hair cells along the tonotopic axis of the cochlea. *Neurosci* **143**, 837–849.
- Fettiplace R & Kim KX (2014). The physiology of mechano-electrical transduction channels in hearing. *Physiol Rev* **94**, 951–986.
- Fettiplace R & Nam JH (2019). Tonotopy in calcium homeostasis and vulnerability of cochlear hair cells. *Hear Res* **376**, 11–21.
- Géléoc GSG, Lennan GW, Richardson GP & Kros CJ (1997). A quantitative comparison of mechano-electrical transduction in vestibular and auditory hair cells of neonatal mice. *Proc Biol Sci* **264**, 611–621.
- Goodyear RJ & Richardson GP (2018). Structure, function, and development of the tectorial membrane: an extracellular matrix essential for hearing. *Curr Top Dev Biol* **130**, 217–244.
- Guinan JJ Jr (1996). Physiology of olivocochlear efferents. In *The Cochlea*, ed. Dallos P, Popper AN, Fay RR, pp. 435–502. Springer, New York.
- Gummer A W, Hemmert W & Zenner HP (1996). Resonant tectorial membrane motion in the inner ear: Its crucial role in frequency tuning. *Proc Natl Acad Sci USA* **93**, 8727–8732.
- He DZ, Jia S & Dallos P (2004). Mechano-electrical transduction of adult outer hair cells studied in a gerbil hemicochlea. *Nature* **429**, 766–770.
- Horner KC (1986). The tensor tympani muscle reflex in the mouse. *Hear Res* **24**, 117–123.
- Ikeda K, Kusakari J & Takasaka T (1988). Ionic changes in cochlear endolymph of the guinea pig induced by acoustic injury. *Hear Res* **32**, 103–110.
- Jeng JY, Johnson SL, Carlton AJ, De Tomasi L, Goodyear RJ, De Faveri F, Furness DN, Wells S, Brown SDM, Holley MC, Richardson GP, Mustapha M, Bowl MR & Marcotti W (2020a). Age-related changes in the biophysical and morphological characteristics of mouse cochlear outer hair cells. *J Physiol* **598**, 3891–3910.
- Jeng JY, Carlton AJ, Johnson SL, Brown SDM, Holley MC, Bowl MR & Marcotti W (2020b). Biophysical and morphological changes in inner hair cells and their efferent innervation in the ageing mouse cochlea. *J Physiol* **599**, 269–287. In press.
- Jeng JY, Ceriani F, Hendry A, Johnson SL, Yen P, Simmons DD, Kros CJ & Marcotti W (2020c) Hair cell maturation is differentially regulated along the tonotopic axis of the mammalian cochlea. *J Physiol* **598**, 151–170.
- Johnson SL, Beurg M, Marcotti W & Fettiplace R (2011). Prestin-driven cochlear amplification is not limited by the outer hair cell membrane time constant. *Neuron* **70**, 1143–1154.
- Johnson SL, Kennedy HJ, Holley MC, Fettiplace R & Marcotti W (2012). The resting transducer current drives spontaneous activity in prehearing mammalian cochlear inner hair cells. *J Neurosci* **32**, 10479–10483.
- Johnson SL, Kuhn S, Franz C, Ingham N, Furness DN, Knipper M, Steel KP, Adelman JP, Holley MC & Marcotti W (2013). Presynaptic maturation in auditory hair cells requires a critical period of sensory-independent spiking activity. *Proc Natl Acad Sci USA* **110**, 8720–8725.
- Johnson SL, Ceriani F, Houston O, Polishchuk R, Polishchuk E, Crispino G, Zorzi V, Mammano F & Marcotti W (2017). Connexin-Mediated Signaling in Nonsensory Cells Is Crucial for the Development of Sensory Inner Hair Cells in the Mouse Cochlea. *J Neurosci* **37**, 258–268.
- Katz E, Elgoyhen AB, Gomez-Casati ME, Knipper M, Vetter DE, Fuchs PA & Glowatzki E (2004). Developmental regulation of nicotinic synapses on cochlear inner hair cells. *J Neurosci* **24**, 7814–7820.
- Kay AR (1992). An intracellular medium formulary. *J Neurosci Methods* **44**, 91–100.
- Kennedy HJ, Evans MG, Crawford AC & Fettiplace R (2003). Fast adaptation of mechano-electrical transducer channels in mammalian cochlear hair cells. *Nat Neurosci* **6**, 832–836.

- Kimura RS (1966). Hairs of the cochlear sensory cells and their attachment to the tectorial membrane. *Acta Oto-Laryngologica* **61**, 55–72.
- Kros CJ, Rüscher A & Richardson GP (1992). Mechano-electrical transducer currents in hair cells of the cultured neonatal mouse cochlea. *Proc Biol Sci* **249**, 185–193.
- Kros CJ, Ruppersberg JP & Rüscher A (1998). Expression of a potassium current in inner hair cells during development of hearing in mice. *Nature* **394**, 281–284.
- Knipper M, Zinn C, Maier H, Praetorius M, Rohbock K, Kopschall I & Zimmermann U (2000). Thyroid hormone deficiency before the onset of hearing causes irreversible damage to peripheral and central auditory systems. *J Neurophysiol* **83**, 3101–3112.
- Kubisch C, Schroeder BC, Friedrich T, Lütjohann B, El-Amraoui A, Marlin S, Petit C & Jentsch TJ (1999). KCNQ4, a novel potassium channel expressed in sensory outer hair cells, is mutated in dominant deafness. *Cell* **96**, 437–446.
- Kujawa SG & Liberman MC (2001). Effects of olivocochlear feedback on distortion product otoacoustic emissions in guinea pig. *J Assoc Res Otolaryngol* **2**, 268–278.
- Legan PK, Lukashkina VA, Goodyear RJ, Kössi M, Russell IJ & Richardson GP (2000). A targeted deletion in alpha-tectorin reveals that the tectorial membrane is required for the gain and timing of cochlear feedback. *Neuron* **28**, 273–285.
- Legan PK, Lukashkina VA, Goodyear RJ, Lukashkin AN, Verhoeven K, Van Camp G, Russell IJ & Richardson GP (2005). A deafness mutation isolates a second role for the tectorial membrane in hearing. *Nat Neurosci* **8**, 1035–1042.
- Legan PK, Goodyear RJ, Morin M, Mencia A, Pollard H, Olavarrieta L, Korchagina J, Modamio-Hoybjør S, Mayo F, Moreno F, Moreno-Pelayo MA & Richardson GP (2014). Three deaf mice: mouse models for TECTA-based human hereditary deafness reveal domain-specific structural phenotypes in the tectorial membrane. *Hum Mol Genet* **23**, 2551–2568.
- Lelli A, Asai Y, Forge A, Holt JR & Géléoc GS (2009). Tonotopic gradient in the developmental acquisition of sensory transduction in outer hair cells of the mouse cochlea. *J Neurophysiol* **101**, 2961–2973.
- Liberman MC, Gao J, He DZ, Wu X, Jia S & Zuo J (2002). Prestin is required for electromotility of the outer hair cell and for the cochlear amplifier. *Nature* **419**, 300–304.
- Luebke AE, Stagner BB, Martin GK & Lonsbury-Martin BL (2015). Influence of sound-conditioning on noise-induced susceptibility of distortion-product otoacoustic emissions. *J Acoust Soc Am* **138**, 58–64.
- Lukashkin AN, Richardson GP & Russell IJ (2010). Multiple roles for the tectorial membrane in the active cochlea. *Hear Res* **266**, 26–35.
- Mahendrasingam S, Beurg M, Fettiplace R & Hackney CM (2010). The ultrastructural distribution of prestin in outer hair cells: a post-embedding immunogold investigation of low-frequency and high-frequency regions of the rat cochlea. *Eur J Neurosci* **31**, 1595–1605.
- Maison SF, Adams JC & Liberman MC (2003). Olivocochlear innervation in the mouse: immunocytochemical maps, crossed versus uncrossed contributions and transmitter colocalization. *J Comp Neurol* **455**, 406–416.
- Mammano F & Nobili R (1993). Biophysics of the cochlea: linear approximation. *J Acoust Soc Am* **93**, 3320–3332.
- Marcotti W & Kros CJ (1999). Developmental expression of the potassium current $I_{K,n}$ contributes to maturation of mouse outer hair cells. *J Physiol* **520**, 653–660.
- Marcotti W, Johnson SL, Holley MC & Kros CJ (2003). Developmental changes in the expression of potassium currents of embryonic, neonatal and mature mouse inner hair cells. *J Physiol* **548**, 383–400.
- Marcotti W, Johnson SL & Kros CJ (2004). A transiently expressed SK current sustains and modulates action potential activity in immature mouse inner hair cells. *J Physiol* **560**, 691–708.
- Marcotti W, van Netten SM & Kros CJ (2005). The aminoglycoside antibiotic dihydrostreptomycin rapidly enters mouse outer hair cells through the mechano-electrical transducer channels. *J Physiol* **567**, 505–521.
- Marcotti W, Corns LF, Goodyear RJ, Rzedzinska AK, Avraham KB, Steel KP, Richardson GP & Kros CJ (2016). The acquisition of mechano-electrical transducer current adaptation in auditory hair cells requires myosin VI. *J Physiol* **594**, 3667–3681.
- Möhrle D, Ni K, Varakina K, Bing D, Lee SC, Zimmermann U, Knipper M & Rüttiger L (2016). Loss of auditory sensitivity from inner hair cell synaptopathy can be centrally compensated in the young but not old brain. *Neurobiol Aging* **44**, 173–184.
- Möhrle D, Reimann K, Wolter S, Wolters M, Varakina K, Mergia E, Eichert N, Geisler HS, Sandner P, Ruth P, Friebe A, Feil R, Zimmermann U, Koesling D, Knipper M & Rüttiger L (2017). NO-sensitive guanylate cyclase isoforms NO-GC1 and NO-GC2 contribute to noise-induced inner hair cell synaptopathy. *Mol Pharmacol* **92**, 375–388.
- Narahari PG, Bhat J, Nambi A & Arora A (2017). Impact of usage of personal music systems on oto-acoustic emissions among medical students. *Noise Health* **19**, 222–226.
- Nowotny M & Gummer AW (2006). Nanomechanics of the subtectorial space caused by electromechanics of cochlear outer hair cells. *Proc Natl Acad Sci U S A* **103**, 2120–2125.
- Oliver D & Fakler B (1999). Expression density and functional characteristics of the outer hair cell motor protein are regulated during postnatal development in rat. *J Physiol* **51**, 791–800.
- Oliver D, Klöcker N, Schuck J, Baukowitz T, Ruppersberg JP & Fakler B (2000). Gating of Ca²⁺-activated K⁺ channels controls fast inhibitory synaptic transmission at auditory outer hair cells. *Neuron* **26**, 595–601.
- Pujol R, Lavigne-Rebillard M & Lenoir M (1998). Development of sensory and neural structures in the mammalian cochlea. In: *Development of the auditory system*. Rubel EW, Popper AN & Fay RR, eds. pp. 146–192. Springer, New York.

- Rau A, Legan PK & Richardson GP (1999). Tectorin mRNA expression is spatially and temporally restricted during mouse inner ear development. *J Comp Neurol* **405**, 271–280.
- Ricci AJ & Fettiplace R (1998). Calcium permeation of the turtle hair cell mechanotransducer channel and its relation to the composition of endolymph. *J Physiol* **506**, 159–173.
- Robertson D & Gummer M (1985). Physiological and morphological characterization of efferent neurones in the guinea pig cochlea. *Hear Res* **20**, 63–77.
- Russell IJ & Sellick PM (1983). Low-frequency characteristics of intracellularly recorded receptor potentials in guinea-pig cochlear hair cells. *J Physiol* **338**, 179–206.
- Rüttiger L, Singer W, Panford-Walsh R, Matsumoto M, Lee SC, Zuccotti A, Zimmermann U, Jaumann M, Rohbock K, Xiong H & Knipper M (2013). The reduced cochlear output and the failure to adapt the central auditory response causes tinnitus in noise exposed rats. *PLoS One* **8**, e57247.
- Salt AN, Inamura N, Thalmann R & Vora A (1989). Calcium gradients in inner ear endolymph. *Am J Otolaryngol* **10**, 371–375.
- Simmons DD, Mansdorf NB & Kim JH (1996). Olivocochlear innervation of inner and outer hair cells during postnatal maturation: evidence for a waiting period. *J Comp Neurol* **370**, 551–562.
- Strimbu CE, Prasad S, Hakizimana P & Fridberger A (2019). Control of hearing sensitivity by tectorial membrane calcium. *Proc Natl Acad Sci USA* **116**, 5756–5764.
- Wood JD, Muchinsky SJ, Filoteo AG, Penniston JT & Tempel BL (2004). Low endolymph calcium concentrations in deafwaddler2J mice suggest that PMCA2 contributes to endolymph calcium maintenance. *J Assoc Res Otolaryngol* **5**, 99–110.
- Wolter S, Möhrle D, Schmidt H, Pfeiffer S, Zelle D, Eckert P, Krämer M, Feil R, Pilz PKD, Knipper M & Rüttiger L (2018). GC-B Deficient Mice With Axon Bifurcation Loss Exhibit Compromised Auditory Processing. *Front Neural Circuits* **12**, 65.
- Zhao DL, Sheppard A, Ralli M, Liu X & Salvi R (2018). Prolonged low-level noise exposure reduces rat distortion product otoacoustic emissions above a critical level. *Hear Res* **370**, 209–216.
- Zheng J, Shen W, He DZ, Long KB, Madison LD & Dallos P (2000). Prestin is the motor protein of cochlear outer hair cells. *Nature* **405**, 149–155.
- Zampini V, Rüttiger L, Johnson SL, Franz C, Furness DN, Waldhaus J, Xiong H, Hackney CM, Holley MC, Offenhauser N, Di Fiore PP, Knipper M, Masetto S & Marcotti W (2011). Eps8 regulates hair bundle length and functional maturation of mammalian auditory hair cells. *PLoS Biol* **9**, e1001048.

Additional information

Data availability statement

The data that support the findings of this study are available from the corresponding authors upon reasonable request.

Competing interests

The authors declare no conflicts of interest.

Author contributions

All authors helped with the collection and analysis of the data. G.P.R. and W.M. conceived and coordinated the study. J.-Y.J., L.R., G.P.R. and W.M. wrote the paper.

All authors approved the final version of the manuscript. All authors agree to be accountable for all aspects of the work in ensuring that questions related to the accuracy or integrity of any part of the work are appropriately investigated and resolved. All persons designated as authors qualify for authorship, and all those who qualify for authorship are listed.

Funding

This work was supported by The Wellcome Trust (102892/Z/13/Z to W.M.; 087737/Z/08/Z to G.P.R.) and Deutsche Forschungsgemeinschaft (DFG: grant SPP 1608 RU 316/12-1 to L.R.). G.P.R. was recipient of a Royal Society Wolfson Merit Award. J.-Y.J. was supported by a PhD studentship from the University of Sheffield. A.J.C. was funded by a PhD studentship from Action on Hearing Loss (S50).

Acknowledgements

We thank C. J. Kros for his critical feedback on an earlier version of the manuscript.

Keywords

adaptation, cochlea, electrophysiology, endolymphatic calcium, hair cells, hearing, mechano-electrical transducer channel, tectorial membrane

Supporting information

Additional supporting information may be found online in the Supporting Information section at the end of the article.

Supplementary Data Set Statistical Summary Document